2. **Liao J, Cui C, Chen S, Ren J, Chen J, et al.** (2009) Generation of induced pluripotent stem cell lines from adult rat cells. Cell Stem Cell 4: 11–15.

3. **Tomioka I, Maeda T, Shimada H, Kawai K, Okada Y, et al.** (2010) Generating induced pluripotent stem cells from common marmoset (Callithrix jacchus) fetal liver cells using defined factors, including Lin28. Genes Cells 15: 959–969.

4. **Liu H, Zhu F, Yong J, Zhang P, Hou P, et al.** (2008) Generation of induced pluripotent stem cells from adult rhesus monkey fibroblasts. Cell Stem Cell 3: 587–590.

5. **Takahashi K, Tanabe K, Ohnuki M, Narita M, Ichisaka T, et al.** (2007) Induction of pluripotent stem cells from adult human fibroblasts by defined factors. Cell 131: 861–872.

6. **Wu Z, Chen J, Ren J, Bao L, Liao J, et al.** (2009) Generation of pig induced pluripotent stem cells with a drug-inducible system. J Mol Cell Biol 1: 46–54.

7. **Wu Y, Zhang Y, Mishra A, Tardif SD, Hornsby PJ** (2010) Generation of induced pluripotent stem cells from newborn marmoset skin fibroblasts. Stem Cell Res 4: 180–188.

8. **Hankowski KE, Hamazaki T, Umezawa A, Terada N** (2011) Induced pluripotent stem cells as a next-generation biomedical interface. Lab Invest 91: 972–977.

9. **Hackett TA, Preuss TM, Kaas JH** (2001) Architectonic identification of the core region in auditory cortex of macaques, chimpanzees, and humans. J Comp Neurol 441: 197–222.

10. **Rogers J, Gibbs RA** (2014) Comparative primate genomics: emerging patterns of genome content and dynamics. Nat Rev Genet 15: 347–359.

11. **Mubiru JN, Yang AS, Olsen C, Nayak S, Livi CB, et al.** (2014) Analysis of prostate-specific antigen transcripts in chimpanzees, cynomolgus monkeys, baboons, and African green monkeys. PLoS One 9: e94522.

12. **Rearden A** (1986) Evolution of glycophorin A in the hominoid primates studied with monoclonal antibodies, and description of a sialoglycoprotein analogous to human glycophorin B in chimpanzee. J Immunol 136: 2504–2509.

13. **Gonzalez JP, Prugnolle F, Leroy E** (2013) Men, primates, and germs: an ongoing affair. Curr Top Microbiol Immunol 365: 337–353.

14. **Wernig M, Meissner A, Foreman R, Brambrink T, Ku M, et al.** (2007) In vitro reprogramming of fibroblasts into a pluripotent ES-cell-like state. Nature 448: 318–324.

15. **Sommer CA, Stadtfeld M, Murphy GJ, Hochedlinger K, Kotton DN, et al.** (2009) Induced pluripotent stem cell generation using a single lentiviral stem cell cassette. Stem Cells 27: 543–549.

16. **Woltjen K, Michael IP, Mohseni P, Desai R, Mileikovsky M, et al.** (2009) piggyBac transposition reprograms fibroblasts to induced pluripotent stem cells. Nature 458: 766–770.

17. **Zhou H, Wu S, Joo JY, Zhu S, Han DW, et al.** (2009) Generation of induced pluripotent stem cells using recombinant proteins. Cell Stem Cell 4: 381–384.

18. **Miyoshi N, Ishii H, Nagano H, Haraguchi N, Dewi DL, et al.** (2011) Reprogramming of mouse and human cells to pluripotency using mature microRNAs. Cell Stem Cell 8: 633–638.

19. **Okita K, Nakagawa M, Hyenjong H, Ichisaka T, Yamanaka S** (2008) Generation of mouse induced pluripotent stem cells without viral vectors. Science 322: 949–953.

20. **Seki T, Yuasa S, Oda M, Egashira T, Yae K, et al.** (2010) Generation of induced pluripotent stem cells from human terminally differentiated circulating T cells. Cell Stem Cell 7: 11–14.

21. **Okita K, Yamakawa T, Matsumura Y, Sato Y, Amano N, et al.** (2013) An efficient nonviral method to generate integration-free human-induced pluripotent stem cells from cord blood and peripheral blood cells. Stem Cells 31: 458–466.

22. **Fusaki N, Ban H, Nishiyama A, Saeki K, Hasegawa M** (2009) Efficient induction of transgene-free human pluripotent stem cells using a vector based on Sendai virus, an RNA virus that does not integrate into the host genome. Proc Jpn Acad Ser B Phys Biol Sci 85: 348–362.

23. **Ban H, Nishishita N, Fusaki N, Tabata T, Saeki K, et al.** (2011) Efficient generation of transgene-free human induced pluripotent stem cells (iPSCs) by temperature-sensitive Sendai virus vectors. Proc Natl Acad Sci U S A 108: 14234–14239.

24. **Hamasaki M, Hashizume Y, Yamada Y, Katayama T, Hohjoh H, et al.** (2012) Pathogenic mutation of ALK2 inhibits induced pluripotent stem cell reprogramming and maintenance: mechanisms of reprogramming and strategy for drug identification. Stem Cells 30: 2437–2449.

25. **Nakagawa M, Takizawa N, Narita M, Ichisaka T, Yamanaka S** (2010) Promotion of direct reprogramming by transformation-deficient Myc. Proc Natl Acad Sci U S A 107: 14152–14157.

26. **Maekawa M, Yamaguchi K, Nakamura T, Shibukawa R, Kodanaka I, et al.** (2011) Direct reprogramming of somatic cells is promoted by maternal transcription factor Glis1. Nature 474: 225–229.

27. **Mali P, Chou BK, Yen J, Ye Z, Zou J, et al.** (2010) Butyrate greatly enhances derivation of human induced pluripotent stem cells by promoting epigenetic remodeling and the expression of pluripotency-associated genes. Stem Cells 28: 713–720.

28. **McLean CY, Reno PL, Pollen AA, Bassan AI, Capellini TD, et al.** (2011) Human-specific loss of regulatory DNA and the evolution of human-specific traits. Nature 471: 216–219.

29. **Langerak AW, Wolvers-Tettero IL, van Dongen JJ** (1999) Detection of T cell receptor beta (TCRB) gene rearrangement patterns in T cell malignancies by Southern blot analysis. Leukemia 13: 965–974.

30. **Nakagawa M, Koyanagi M, Tanabe K, Takahashi K, Ichisaka T, et al.** (2008) Generation of induced pluripotent stem cells without Myc from mouse and human fibroblasts. Nat Biotechnol 26: 101–106.

31. **Stadtfeld M, Nagaya M, Utikal J, Weir G, Hochedlinger K** (2008) Induced pluripotent stem cells generated without viral integration. Science 322: 945–949.

32. **Soldner F, Hockemeyer D, Beard C, Gao Q, Bell GW, et al.** (2009) Parkinson's disease patient-derived induced pluripotent stem cells free of viral reprogramming factors. Cell 136: 964–977.

33. **Nagai Y TA, Irie T, Yonemitsu Y, Gotoh B** (2011) Sendai virus: Evolution from mouse pathogen to a state-of-the-art tool in virus research and biotechnology. The biology of Paramyxoviruses Samal SK, Ed, Caister Academic Press, Norfolk, UK: 115–173.

34. **Kehrer-Sawatzki H, Cooper DN** (2007) Understanding the recent evolution of the human genome: insights from human-chimpanzee genome comparisons. Hum Mutat 28: 99–130.

35. **Marchetto MC, Narvaiza I, Denli AM, Benner C, Lazzarini TA, et al.** (2013) Differential L1 regulation in pluripotent stem cells of humans and apes. Nature 503: 525–529.

36. **Sasaki K, Inoue M, Shibata H, Ueda Y, Muramatsu SI, et al.** (2005) Efficient and stable Sendai virus-mediated gene transfer into primate embryonic stem cells with pluripotency preserved. Gene Ther 12: 203–210.

37. **Fusaki N BH, Nagai Y** (2014) Induction of Human Pluripotent Stem Cells by the Sendai Virus Vector: Establishment of a Highly Efficient and Footprint-Free System. Sendai Virus Vector: Advantages and Applications Springer 171–183.

38. **Kitagawa M, Takebe A, Ono Y, Imai T, Nakao K, et al.** (2012) Phf14, a novel regulator of mesenchyme growth via platelet-derived growth factor (PDGF) receptor-alpha. J Biol Chem 287: 27983–27996.

39. **Sakurai H, Era T, Jakt LM, Okada M, Nakai S, et al.** (2006) In vitro modeling of paraxial and lateral mesoderm differentiation reveals early reversibility. Stem Cells 24: 575–586.

40. **Yan Y, Shin S, Jha BS, Liu Q, Sheng J, et al.** (2013) Efficient and rapid derivation of primitive neural stem cells and generation of brain subtype neurons from human pluripotent stem cells. Stem Cells Transl Med 2: 862–870.

CellPress

Cell Metabolism
Article

Methionine Metabolism Regulates Maintenance and Differentiation of Human Pluripotent Stem Cells

Nobuaki Shiraki,[1,8] Yasuko Shiraki,[2,8] Tomonori Tsuyama,[1,3] Fumiaki Obata,[4,5] Masayuki Miura,[4,5] Genta Nagae,[6] Hiroyuki Aburatani,[6] Kazuhiko Kume,[1,7] Fumio Endo,[2,*] and Shoen Kume[1,3,*]

[1]Department of Stem Cell Biology, Institute of Molecular Embryology and Genetics, Kumamoto University, Honjo 2-2-1, Kumamoto 860-0811, Japan

[2]Department of Pediatrics, Graduate School of Medical Sciences, Kumamoto University, Honjo 1-1-1, Kumamoto 860-8556, Japan

[3]Program for Leading Graduate Schools "HIGO," Kumamoto University, Honjo 2-2-1, Kumamoto 860-0811, Japan

[4]Department of Genetics, Graduate School of Pharmaceutical Sciences, The University of Tokyo, Hongo 7-3-1, Bunkyo-ku, Tokyo 113-0033, Japan

[5]CREST, Japan Science and Technology Agency, Chiyoda-ku, Tokyo 102-0075, Japan

[6]Genome Science Division, Research Center for Advanced Science and Technology, The University of Tokyo, Komaba 4-6-1, Meguro-ku, Tokyo 153-8904, Japan

[7]Department of Neuropharmacology, Graduate School of Pharmaceutical Sciences, Nagoya City University, 3-1 Tanabe-dori, Mizuho-ku, Nagoya 467-8603, Japan

[8]Co-first authors

*Correspondence: fendo@kumamoto-u.ac.jp (F.E.), skume@kumamoto-u.ac.jp (S.K.)

http://dx.doi.org/10.1016/j.cmet.2014.03.017

SUMMARY

Mouse embryonic stem cells (ESCs) and induced pluripotent stem cells (iPSCs) are in a high-flux metabolic state, with a high dependence on threonine catabolism. However, little is known regarding amino acid metabolism in human ESCs/iPSCs. We show that human ESCs/iPSCs require high amounts of methionine (Met) and express high levels of enzymes involved in Met metabolism. Met deprivation results in a rapid decrease in intracellular S-adenosylmethionine (SAM), triggering the activation of p53-p38 signaling, reducing NANOG expression, and poising human iPSC/ESCs for differentiation, follow by potentiated differentiation into all three germ layers. However, when exposed to prolonged Met deprivation, the cells undergo apoptosis. We also show that human ESCs/iPSCs have regulatory systems to maintain constant intracellular Met and SAM levels. Our findings show that SAM is a key regulator for maintaining undifferentiated pluripotent stem cells and regulating their differentiation.

INTRODUCTION

Embryonic stem cells (ESCs) and induced pluripotent stem cells (iPSCs) have an unlimited ability to replicate; they are pluripotent and can give rise to all cell types. ESCs/iPSCs possess a unique transcriptional circuit that sustains the pluripotent state. These cells are in a specific epigenetic state that is ready for rapid cell-fate decisions. Furthermore, various forms of histone methylation allow dynamic regulation of ESC/iPSC pluripotency and plasticity. ESCs/iPSCs also possess a characteristically high rate of proliferation as well as an abbreviated G1 phase. These unique molecular properties distinguish ESCs and iPSCs from somatic cells (Boheler, 2009).

These unusual features signify that ESCs/iPSCs exist in a specialized metabolic state. ESCs and iPSCs rely specifically on glycolysis (Armstrong et al., 2010; Facucho-Oliveira and St John, 2009), whereas somatic cells utilize mitochondrial oxidative phosphorylation for energy production. This metabolic requirement appears to play a causative role rather than being a consequence of pluripotency acquisition (Folmes et al., 2011). Recent reports have shown that metabolism is tightly linked to cellular signaling, and these two processes reciprocally regulate each other and modulate cell activities such as cell survival, proliferation, and stem cell function (Takubo et al., 2013; Wellen and Thompson, 2012).

Mouse ESCs are in a high-flux metabolic state, with a high dependence on threonine (Thr) catabolism (Alexander et al., 2011; Wang et al., 2009). It was recently reported that Thr metabolism regulates intracellular S-adenosylmethionine (SAM) and histone methylation such that depletion of Thr from the culture medium or knockdown of threonine dehydrogenase (*Tdh*) in mouse ESCs decreases SAM accumulation and trimethylation of histone H3 lysine 4 (H3K4me3), leading to slowed growth and increased differentiation (Shyh-Chang et al., 2013). However, in human cells, *Tdh* is expressed as a nonfunctional pseudogene. Furthermore, little is known regarding amino acid metabolism and its role in human ESCs/iPSCs. These reports highlight the importance of examining the metabolic state of human ESCs/iPSCs, which may improve our understanding of the signaling pathways regulating cell survival, pluripotency maintenance, and differentiation.

Methionine (Met) is an essential amino acid (Finkelstein, 1990). An important metabolite of Met is SAM, which is produced through an intermediate reaction catalyzed by methionine

adenosyltransferase (MAT). There are three major multimeric MAT enzymes: MATI, MATII, and MATIII (Halim et al., 1999). MATI is a tetramer and MATIII is a dimer of the protein encoded by *MAT1A*, whereas MATII is a dimer of the protein encoded by *MAT2A*. SAM is a methyl donor crucial for gene regulation (Lu and Mato, 2008). DNA methylation and protein methylation, including histone methylation, are catalyzed by methyltransferases by using SAM as a methyl donor (Goll and Bestor, 2005; Shi, 2007). S-adenosylhomocysteine (SAH) is generated as a product of transmethylation by methyltransferases such as DNA methyltransferases (DNMTs) and is then converted to homocysteine (Hcy) by SAH hydrolase (AHCY). Hcy is remethylated and converted to Met by 5-methyltetrahydrofolate-homocysteine methyltransferase (MTR), which requires folate and vitamin B12 or betaine-homocysteine methyltransferase (BHMT) as a methyl donor. Alternatively, Hcy is converted to cystathionine by cystathionine β-synthase (CBS) and then further metabolized to cysteine by cystathionase (CTH). The Met salvage pathway, in which S-methyl-5′-thioadenosine (MTA), a byproduct of polyamine biosynthesis, is enzymatically converted to Met through several enzymatic steps, is also involved in Met metabolism. However, no study yet has focused on the Met salvage pathway in human ESCs/iPSCs.

Here, we show that undifferentiated pluripotent human ESCs/iPSCs are in a high-Met metabolic state that decreased with differentiation. We examined the underlying mechanisms and measured metabolites.

RESULTS

Met Deprivation Causes Cell-Cycle Arrest and Impairment of Survival in Pluripotent Human ESCs/iPSCs

We first deprived single amino acids from the culture medium for 48 hr during culture of the undifferentiated human ESC line khES3 (Suemori et al., 2006) and the human iPSC line 201B7 (Takahashi et al., 2007), and we examined their impact on cell survival (Figure 1A). Deprivation of leucine (Leu), lysine (Lys), tryptophan (Trp), or Met resulted in inhibition of cell growth and decreased cell number (Figure 1A). Bright-field microscopy showed cell death when cells were grown in Leu-, Lys-, or Met-deprived conditions (Figure S1 available online). Met deprivation was the most effective growth inhibitor of human pluripotent stem cells; we therefore focused on Met.

When Met concentration in the media was reduced from 120 μM to 12 μM, self-renewal was reduced in both khES3 and 201B7 cells (Figure 1B). Similar results were observed with other human ESC (khES1) or iPSC (253G1) lines (Figure S1B). Time-dependent studies revealed a significant reduction in cell number (Figure 1C) and self-renewal (Figure 1D) as early as 5 hr after Met deprivation. Apoptosis significantly increased after 24 hr of Met deprivation (Figure 1E), and at 48 hr more than half of the cells were TUNEL-positive (Figure 1E). Apoptosis was also observed with Leu or Lys deprivation in khES3 cells (Figure S1C).

G0/G1 phase arrest, as well as a reduction in the cell population in S and G2/M phases, was observed following prolonged Met deprivation for 24 hr in both khES3 and 201B7 cells (Figure 1F). G0/G1 phase arrest was also observed after Leu and Lys deprivation for 48 hr (Figure S1D).

These results indicate that undifferentiated human ESCs/iPSCs require greater than 25 μM Met for maintenance and that deprivation of Met results in growth inhibition, followed by cell-cycle arrest and cell death.

Rapid Decrease in Intracellular SAM and MTA Levels and Cessation of Hcy Excretion after Met Deprivation

In mouse ESCs, Thr is essential for cell growth, and deprivation of Thr reduces intracellular SAM ($[SAM]_i$) levels (Shyh-Chang et al., 2013). To determine the intracellular level of Met ($[Met]_i$) and its metabolites in human ESCs/iPSCs cultured in complete (control) or Met-deprived conditions, we analyzed and quantified intracellular Met-cycle metabolites (Met, SAM, SAH, and MTA) and excreted Hcy in khES3 and 201B7 cells. The $[Met]_i$ level decreased 5 and 24 hr after Met deprivation (Figure 2A, Met). We observed a decrease in $[SAM]_i$ and $[MTA]_i$ at 5 hr, which increased 24 hr after Met deprivation, with $[SAM]_i$ returning to a level similar to that of the control (Figure 2A, SAM). MTA supplementation increased $[Met]_i$ in both control and Met-deprived conditions (Figure 2A, Met). This result suggests that human ESCs actively convert MTA into Met, and then into SAM, even in complete media. This preference of SAM and MTA utilization explains the early decrease in $[SAM]_i$ and $[MTA]_i$ at 5 hr after Met deprivation. Interestingly, a rapid release of intracellular Hcy into the media was observed in complete media (Figure 2B). Hcy excretion was not seen under Met deprivation conditions, which reoccurred when supplemented with MTA. We interpreted this result to indicate conversion of MTA into Met, which then entered the Met cycle with subsequent metabolization into Hcy. Decreased SAM and cessation of Hcy excretion were also observed in 201B7 cells (Figures 2C and 2D).

Expression profile analysis revealed that Met depletion triggered a marked downregulation of Met metabolic enzymes, including *DNMT3B* (Figures 2E and 2F). While *MAT2A*, which catalyzes the conversion of Met into SAM in pluripotent stem cells, significantly increased under Met deprivation, *MAT2B* expression was attenuated under Met deprivation, showing a rapid decrease and a later increase after 10 hr. It is possible that *MAT2A*/*MAT2B* upregulation may then lead to an increase in $[SAM]_i$ (Figure 2A, SAM).

SAM Is Crucial for Self-Renewal and Survival of Human ESCs/iPSCs

To examine the role of Met metabolism in self-renewal of human ESCs/iPSCs, we performed Met deprivation and rescue by supplementation with Met metabolites such as Met itself, SAM, Hcy, or MTA. In both khES3 and 201B7 cells, cell death induced by Met deprivation was rescued by supplementation with Met, SAM, Hcy, or MTA (Figure 3A). Met supplementation was the most effective, followed by SAM and MTA supplementation. Hcy supplementation showed limited rescue effects compared to Met. MTA supplementation also rescued cell depletion, confirming the conversion of MTA to Met through the salvage cycle (Figure 2).

These results suggest the importance of Met and SAM for maintaining ESC/iPSC self-renewal. To examine whether Met or SAM is essential for the maintenance of pluripotent stem cells, we performed knockdown of *MAT2A*, *MAT2B*, and spermine synthase (*SMS*) (Figures 3B and 3C). Knockdown of *MAT2A* or

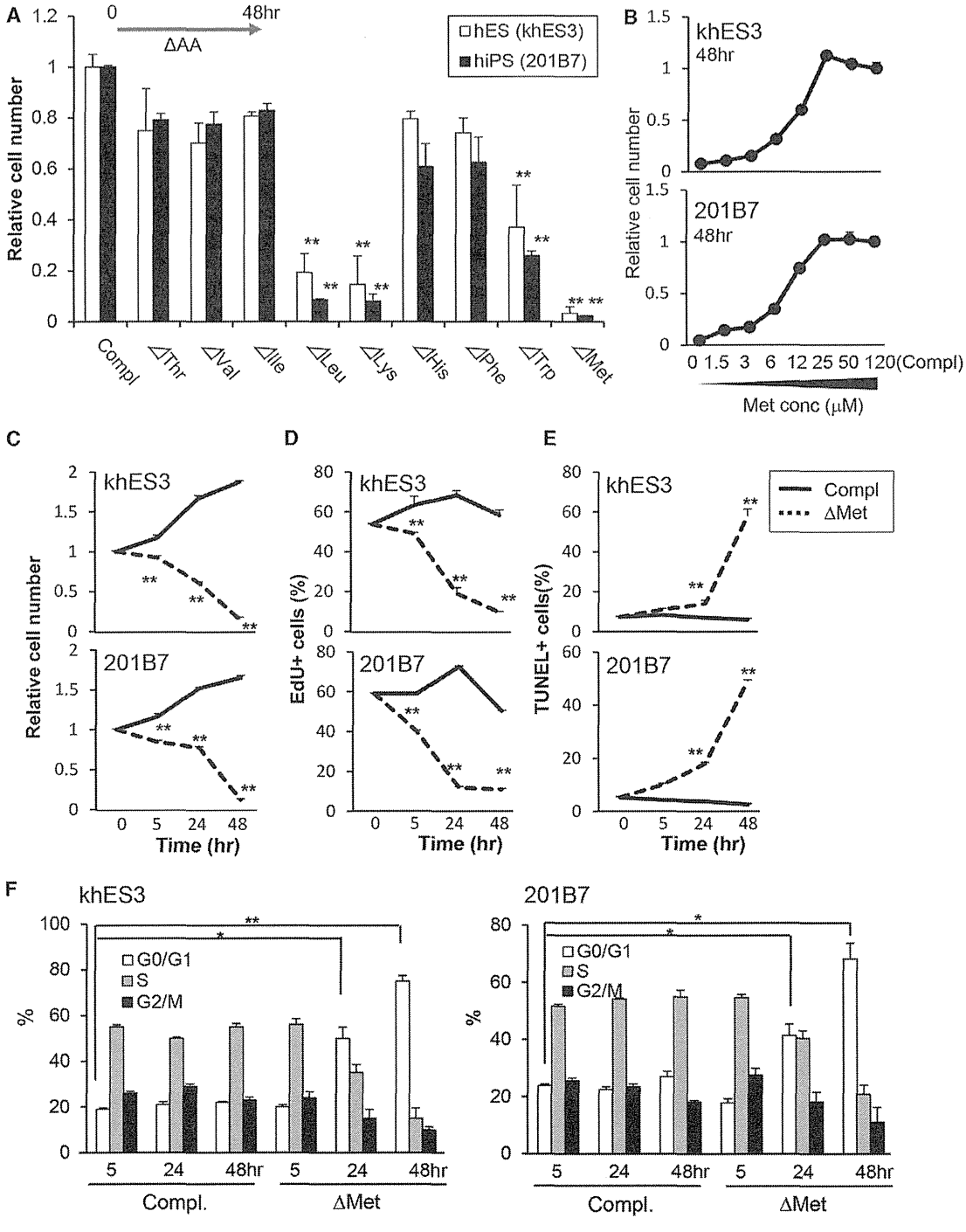

Figure 1. Impact of Met Deprivation on Undifferentiated Human ESCs/iPSCs

(A) Total number of undifferentiated khES3 (open bars) and 201B7 (black bars) cells after 48 hr amino acid deprivation.

(B–F) Shown are graded Met concentration (B) and time-dependent effects on total cell number (C), proliferation (D), apoptosis (E), and G0/G1 arrest (F). Error bars, SEM (n = 3). Significant differences were determined by Student's t test; *p < 0.05 and **p < 0.01.

MAT2B, but not *SMS*, decreased self-renewal (Figures 3B, 3C, and S2). Rescue of self-renewal by SAM addition was not affected by *SMS* knockdown (Figure 3C). The above results indicate that SAM, rather than Met itself, is essential for self-renewal and survival (Figures 3B and 3C).

Next, the effect of cycloleucine, an analog of Met that acts as a specific inhibitor of MAT (Sufrin et al., 1979), was tested. khES3 and 201B7 cells treated with increasing cycloleucine for 48 hr showed a significant decrease in cell number at 100 mM cycloleucine (Figure 3D). Cycloleucine treatment for 24 hr significantly

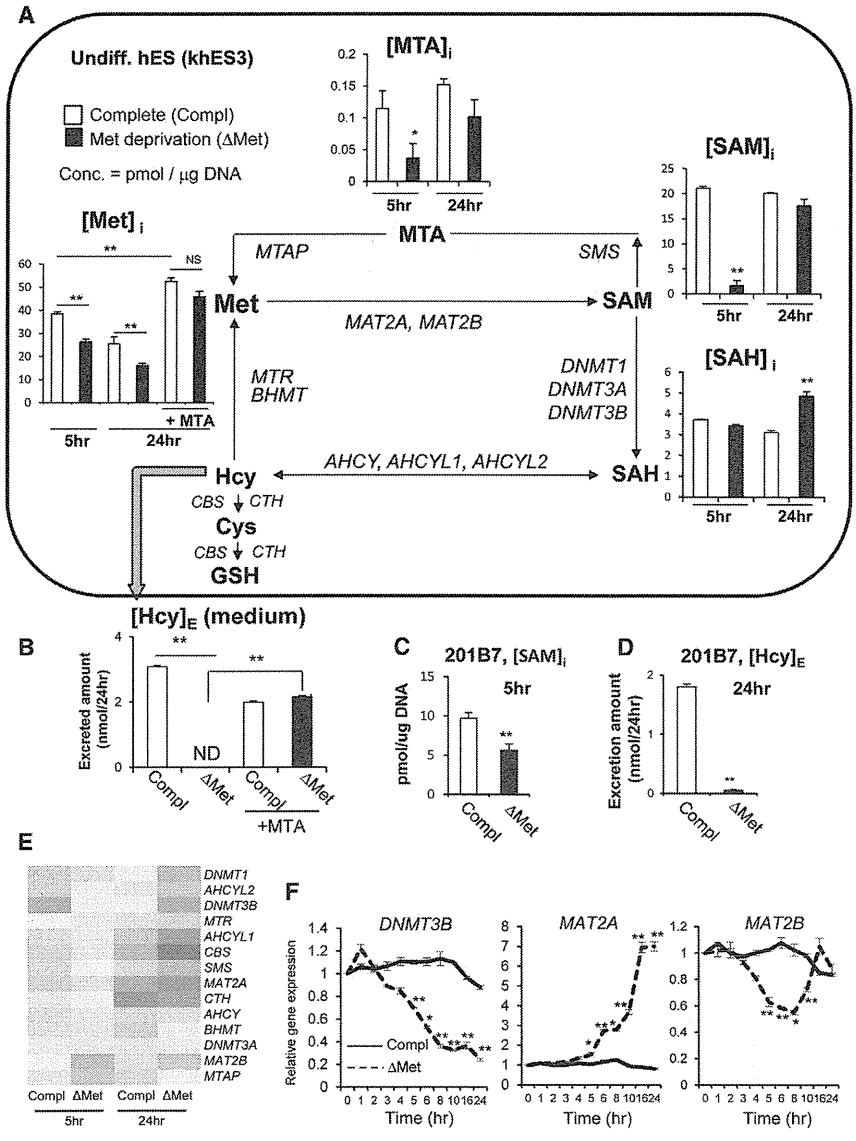

Figure 2. Measurement of Met-Cycle Metabolites

(A) Intracellular concentration of Met ($[Met]_i$), MTA ($[MTA]_i$), SAM ($[SAM]_i$), and SAH ($[SAH]_i$) in undifferentiated khES3 cells 5 and 24 hr after culture in complete (open bars) or Met-deprived (black bars) media, normalized to DNA.

(B) Hcy excretion ($[Hcy]_E$) in khES3 cells 24 hr after Met deprivation. ND, not detected.

(C) $[SAM]_i$ of undifferentiated 201B7 cells after 5 hr culture in complete (open bars) or Met-deprived (black bars) media.

(D) $[Hcy]_E$ in 201B7 cells after 24 hr culture.

(E) Expression profiles of Met-Cys metabolic enzymes in undifferentiated khES3 cells cultured in complete or Met-deprived (ΔMet) media for 5 or 24 hr.

(F) Time-dependent changes in levels of *DNMT3B*, *MAT2A*, and *MAT2B* by real-time PCR. Error bars represent SEM (n = 3). Significant differences were determined by Student's t test; NS, no significance, *$p < 0.05$, and **$p < 0.01$.

lowered $[SAM]_i$ without affecting $[Met]_i$ or $[SAH]_i$ (Figure 3E), demonstrating that SAM, but not Met, is essential for the self-renewal and survival of human ESCs/iPSCs.

Next, to examine how prolonged Met deprivation affects cell survival, we performed 5 hr and 24 hr Met deprivation studies (Figure 3F) followed by 48 hr of culture in complete or Met-deprived media in khES3 and 201B7 cells. Deprivation of Met for 5 hr was reversible, and cells proliferated after switching to complete media (Figure 3F, c). However, under prolonged (24 hr) Met deprivation, cell proliferation did not recover even when cells were switched to complete media (Figure 3F, f). This result suggests that a short Met deprivation is reversible, but prolonged Met deprivation is vital for cell survival. Considering that intracellular Met metabolite concentrations change with time (Figure 2), our results suggest that SAM may act as an early sensor. Met deprivation led to SAM reduction and decreased proliferation, and prolonged Met deprivation resulted in G0/G1 phase cell-cycle arrest (Figure 1F), which then led to apoptosis.

Met Deprivation in Undifferentiated Human ESCs/iPSCs Induced Upregulation of the p53-p38 Signaling Pathway, which Is Critical for Cell-Cycle Arrest and Apoptosis

We next attempted to identify the signaling pathway responsible for the impaired cell survival. We performed gene expression profiles of undifferentiated khES3 cells cultured in complete or Met-deprived conditions for 5 or 24 hr. Cell-cycle- and apoptosis-related genes increased by >3-fold (Figure 4A) and >2-fold (Table S1A), respectively, in the Met-deprived group compared to the complete control. Significant increases were observed in levels of p53-dependent genes involved in apoptosis, such as *ATM*, *ATR*, *MDM2*, *CDKN1A*, *FAS*, *TNFRSF10A*, and *TNFRSF10D*. Additionally, Met deprivation for 24 hr increased *CASP3* and *CASP8*, which are critical mediators of apoptosis (Figure 4A). Enrichment analysis identified signaling pathways, the expression levels of which increased by >3-fold at 5 or 24 hr Met deprivation, are shown in Table S1B.

Because transcript levels of *p53* were unchanged under Met deprivation conditions, we next examined p53 at the protein level. Total p53 protein increased within 5 hr of Met deprivation in both khES3 and 201B7 cells, detected by western blot (Figure 4B) and immunocytochemical analyses (Figure 4C). Supplementation of Met decreased the proportion of $p53^+$ cells in a concentration-dependent manner (Figure 4D). Interestingly, the increase in $p53^+$ cells was observed specifically under Met deprivation, but not under deprivation of other amino acids (Figure 4E). Moreover, p53 upregulation was completely abolished by SAM supplementation (Figure 4E, ΔMet+SAM) and triggered by cycloleucine (Figure 4F). To determine the effect of ΔMet-induced p53 on cell death in khES3 cells, we performed knockdown of *p53*

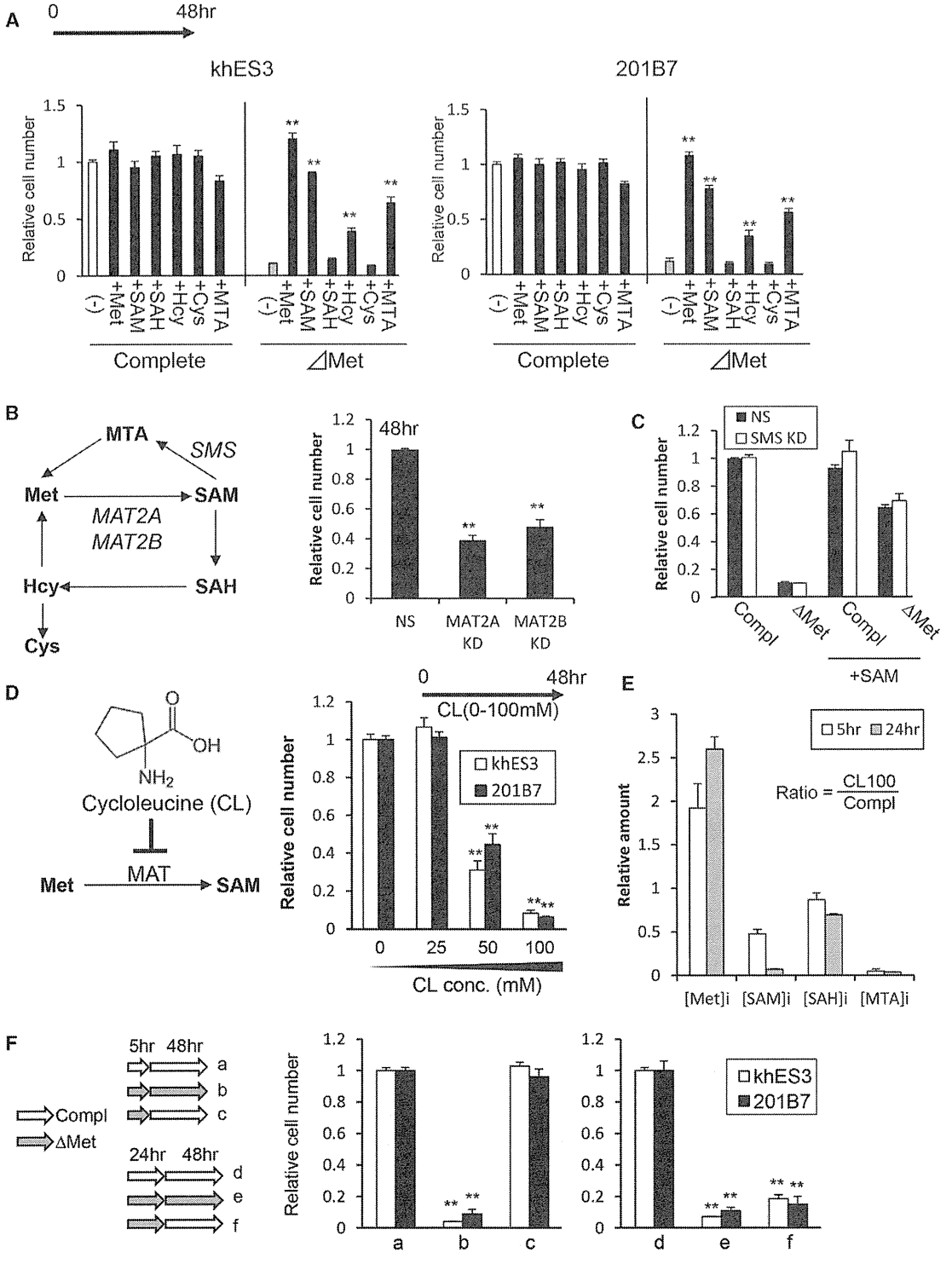

Figure 3. Met Metabolism Is Crucial for Human ESC/iPSC Proliferation

(A) Quantitative analyses of relative khES3 (left panels) and 201B7 (right panels) cell numbers after culture for 48 hr in complete or Met-deprived (ΔMet) media. Cells were supplemented with 100 μM Met, SAM, SAH, Hcy, Cys, or MTA (black bars), and cell numbers were compared with the control complete media (white bars).

(B) Relative cell numbers of nonsilenced (NS), *MAT2A*, or *MAT2B* KD khES3 cells 48 hr after knockdown.

(C) Quantitative analyses of relative cell numbers of NS or *SMS* KD khES3 cells after 48 hr culture in complete or Met-deprived (ΔMet) media. Supplementation of 100 μM SAM (+SAM).

(legend continued on next page)

(p53 KD) in khES3 cells. Upregulation of p53 and phosphorylated p38 (p-p38), a downstream target of p53, were not observed in p53 KD cells 5 hr after Met deprivation (Figure 4G). p53 KD cells showed a partial rescue of the cell death induced by 48 hr Met deprivation (Figure 4H). Moreover, khES3 cells treated with a p38 inhibitor, SB239063 (SB), also showed a partial rescue of the cell death caused by Met deprivation (Figure 4I).

Our results indicate that activation of the p53-p38 signaling pathway is an early response at 5 hr, induced by Met deprivation. p38 activation partially accounts for the cell-cycle arrest, which leads to apoptosis of undifferentiated human ESCs/iPSCs upon prolonged Met deprivation.

Genes that were upregulated after Leu and Lys deprivation for 5 hr, but not after Met deprivation, were also identified (Figure S3A, Table S1C). Among these, DNA damage-inducible transcript 3 (*DDIT3*) increased significantly by real-time PCR analysis (Figure S3B). DDIT3, also known as C/EBP homologous protein (CHOP) and growth arrest and DNA damage-inducible gene 153 (GADD153), is an important component of the endoplasmic reticulum (ER) stress-mediated apoptosis pathway (Oyadomari and Mori, 2004). DDIT3 is induced by Leu depletion in human cell lines (Bruhat et al., 1997). These results, therefore, suggest that Leu and Lys deprivation induced apoptosis (Figure 1) through a mechanism different from that of Met deprivation.

Met Deprivation Reduced Histone and DNA Methylation, Decreased NANOG Expression, and Increased Overall Differentiation Potency

Our results showed that $[SAM]_i$ decreased rapidly within 5 hr of Met deprivation (Figure 2) and that treatment with SAM rescued Met deprivation-induced cell death (Figure 3A) and abolished upregulation of p53 (Figure 4E). SAM functions as a major methyl donor in methyl transfer reactions, such as methylation of histone H3 K4, K9, K27, and K36 and DNA methylation. A study in mouse ESCs demonstrated that SAM reduction decreased H3K4me3 (Shyh-Chang et al., 2013), but the effect of SAM reduction on epigenetic modifications of human ESCs/iPSCs is unknown. We thus examined the impact of Met deprivation on histone (Figures 5A and 5B) and DNA methylation (Figure 5C). After short-term (5 hr) Met deprivation in undifferentiated 201B7 cells, a rapid decrease in H3K4me3 was observed, which was reversed by the addition of SAM. Cycloleucine (100 mM) also decreased trimethylation of H3K4me3 levels (Figure 5A). Decreased H3K4me3 was also observed in khES3 cells (Figure 5B) and persisted under long-term (24 hr) Met deprivation (Figures 5A and 5B). Therefore, H3K4me3 demethylation occurred as a rapid response to decreased $[SAM]_i$ in human ESCs/iPSCs, similar to mouse ESCs. We also compared the extent of DNA methylation in undifferentiated 201B7 cells cultured for 5 hr in Met-deprived and complete media. A modest reduction in global DNA methylation was observed (Figure 5C), with 1,864 probes showing a decrease in Met-deprived cells greater than 15%, compared to those cultured in complete medium. Affected regions were not located at transcriptional start sites (TSSs) but were primarily in the vicinities of TSSs or gene body regions (Figure 5C). However, we could not identify specific genes regulated by Met deprivation (N.S., unpublished data). Taken together, our results indicate that Met deprivation results in a decrease in $[SAM]_i$, leading to a reduction in H3K4me3 and a global reduction in DNA methylation in human ESCs/iPSCs.

Decreased $[SAM]_i$ occurred 5 hr after Met deprivation and triggered p53-p38 activation (Figure 4). As p53 has been reported to induce differentiation of mouse ESCs by suppressing Nanog expression (Lin et al., 2005), we examined whether expression of pluripotent markers was affected. We found that NANOG expression decreased in undifferentiated 201B7 and khES3 cells after Met deprivation, while OCT3/4 expression was unaffected (Figures 5D and 5E). We next examined whether deprivation of other amino acids had an effect on *NANOG* and *OCT3/4* expression, and we found that Leu deprivation also triggered a decrease in *NANOG* expression, although to a level lower than that of Met deprivation. The decrease in *NANOG* expression was rescued by supplementation with Met or SAM in a concentration-dependent manner (Figures 5G and 5H).

We then tested whether a short period of Met deprivation increased the differentiation potency of human iPSCs (Figures 5I–5K). Pluripotent 201B7 cells were cultured in Met-deprived maintenance media for 10 hr and then subjected to differentiation into the definitive endoderm. The proportion and total number of $SOX17^+$ definitive endoderm cells increased in the Met-deprived group compared to the control group at differentiation day 4 (D4), indicating that Met deprivation potentiated differentiation into definitive endoderm (Figure 5I). However, gene expression profiling did not show marked induction of differentiation markers after Met deprivation at 5 or 24 hr (Figure S4A), suggesting that exposure to induction signals is required for triggering differentiation. Similar results were observed in khES1, khES3, and 253G1 iPSCs, indicating that potentiation of differentiation was commonly observed across different human ESC/iPSC lines (Figures S4B–S4D).

We then examined whether potentiation of differentiation occurs with differentiation into other germ layers. Undifferentiated 201B7 cells were cultured under Met-deprived conditions and then directed toward mesoderm differentiation. We observed a higher proportion of cells expressing the early mesoderm marker T protein (Figure 5J). Similarly, when deprived of Met and then directed to differentiate into ectodermal and neuronal lineages, expression levels of *PAX6* or *MAP2* increased compared to those cultured in complete media (Figure 5K).

Taken together, our results indicate that a short exposure to Met deprivation of undifferentiated human iPSCs decreased NANOG expression and increased the overall differentiation potency into the three germ layers.

(D) Relative khES3 (open bars) and 201B7 (black bars) cell numbers after culture for 48 hr in complete media with 0, 25, 50, or 100 mM cycloleucine (CL).
(E) Intracellular Met ([Met]i), SAM ([SAM]i), SAH ([SAH]i), and MTA ([MTA]i) levels in undifferentiated khES3 cells 5 hr (open bars) or 24 hr (gray bars) after culture in complete or 100 mM cycloleucine (CL100) media are shown. Data are normalized to DNA, and relative metabolite amounts are shown as a ratio of values at CL100 versus complete media.
(F) Relative cell numbers of cells treated for different time periods under control complete and Met-deprived conditions as shown in conditions a–c and d–f. Error bars represent SEM (n = 3). Significant differences compared to nonsupplemented cells (a and d) were determined by Student's t test; $^{**}p < 0.01$.

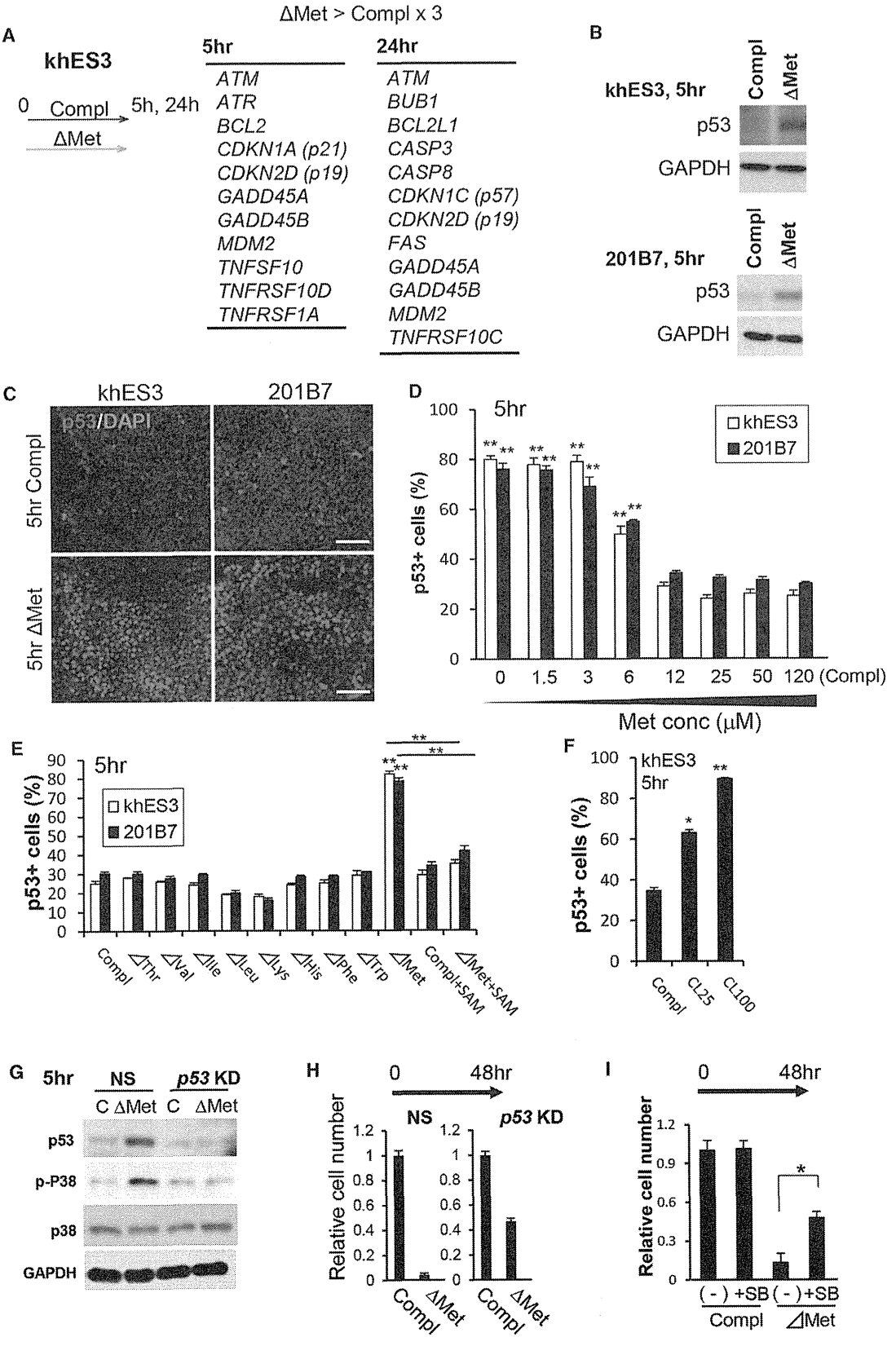

(legend on next page)

Undifferentiated Human ESCs Are in a High-Met Metabolic State Compared to Differentiated Cells

We previously established a procedure for inducing ESCs sequentially into the definitive endoderm as well as specific digestive organs, such as the pancreas, liver, and intestines (Ogaki et al., 2013; Shiraki et al., 2008a, 2008b, 2011). Marked differences exist in the differentiation potencies of human ESC/iPSC lines, which is an issue for efficient directed differentiation of human ESCs/iPSCs in vitro (Kajiwara et al., 2012; Osafune et al., 2008). We thus investigated differences in Met metabolism upon human ESC differentiation by focusing differentiation into the endoderm lineages.

We examined gene expression profiles, Met consumption, and Hcy excretion using undifferentiated khES3 cells, and the derived definitive endoderm cells differentiated under feeder-free conditions (Iwashita et al., 2013) (Figure 6A). Microarray analysis indicated that expression of essential Met and Cys metabolic enzymes, such as *DNMT*, was high in undifferentiated khES3 cells (Figure 6B). *MAT2A* expression was also elevated in undifferentiated khES3 cells, but downregulated in the definitive endoderm, whereas *MAT2B* levels were unchanged (Figure 6B).

The concentration of Met in the media rapidly decreased during maintenance culture, due to cellular uptake (Figure 6C). Total consumption of Met was significantly lower when cells adopted definitive endoderm differentiation compared to undifferentiated human ESCs. Furthermore, Hcy excretion from the endoderm was low and unaffected by Met deprivation (Figure 6D).

These results indicate that undifferentiated khES3 cells are in a high-flux Met metabolic state. In contrast, endoderm cells require a low amount of Met for cell growth and therefore are not affected by Met deprivation. This metabolic difference between undifferentiated cells and endoderm cells prompted us to test the effects of Met deprivation on eliminating remaining undifferentiated cells during differentiation.

Long-Term Met Deprivation Leads to Apoptosis, Specifically in Undifferentiated Cells, and Potentiates Endoderm and Hepatic Differentiation

Definitive endoderm differentiations of human ESC lines khES1 and khES3, and human iPSC lines 201B7 and 253G1 on day 10 (D10), are shown in Figure 7 (Shiraki et al., 2008a; Umeda et al., 2013). When khES3 or 253G1 cells were differentiated into definitive endoderm, OCT3/4 expression was rapidly downregulated. In contrast, in khES1 or 201B7 cells, a higher proportion of OCT3/4-expressing undifferentiated cells remained at D10 (Figure 7A). For hepatic differentiation, media was changed to hepatocyte differentiation media at D10 (Shiraki et al., 2008a; Umeda et al., 2013). The remaining undifferentiated cells were an obstacle for further differentiation, and expression of the early liver marker *AFP* and the hepatocyte marker albumin (*ALB*) in 201B7 cells was lower than that in khES3-derived differentiated cells (Figure 7B). Because Met deprivation triggered cell death in undifferentiated cells (Figure 1) without affecting Met metabolism in the definitive endoderm (Figure 6D), we deprived Met during mid-stage endoderm differentiation from day 8 (D8) to D10 in 201B7 cells. Met deprivation eliminated the undifferentiated OCT3/4 cells without affecting $SOX17^+$ cells (Figure 7C). We also tested khES1 cells, which are resistant to endoderm differentiation. Met deprivation also improved the differentiation efficiency of khES1 cells by eliminating undifferentiated cells (Figure 7D). Next, we analyzed the impact of Met deprivation on apoptosis. TUNEL-positive cells significantly increased with Met deprivation, which was observed in $OCT3/4^+$ cells, but not in $SOX17^+$ cells (Figure 7E). Quantitative measurements revealed that a high percentage of $OCT3/4^+$ cells (60%), but not $SOX17^+$ cells, rapidly became apoptotic upon Met deprivation (Figure 7F). As Met deprivation promoted cell death only in undifferentiated cells, we next examined its impact on hepatic differentiation. Met deprivation during D8–10 (Figures 7G–7I) potentiated the differentiation of 201B7 cells into the hepatic lineage, resulting in a remarkable increase in the proportion of AFP^+ cells and a reduction in $OCT3/4^+$ cells (Figure 7G). Met deprivation in 201B7 cells resulted in increased expression of *ALB* to a level even higher than that in primary hepatocytes (pHep) (Figure 7H), and secretion of ALB was higher than that in pHep as well (Figure 7I).

These data indicate that prolonged Met deprivation eliminates residual undifferentiated cells and leads to an increased overall differentiation efficiency in resistant cell lines, with respect to differentiation into endoderm and hepatic lineages.

DISCUSSION

In contrast to mouse ESCs, which are highly dependent on Thr metabolism, Tdh is nonfunctional in humans; moreover, we observed that undifferentiated pluripotent ESCs/iPSCs were in a high-Met metabolic state. We also found that SAM is required for the self-renewal of human ESCs/iPSCs and maintenance of an undifferentiated state. Short-term depletion of SAM triggered the following: (i) demethylation of H3K4me3, (ii) global DNA demethylation, (iii) p53 signaling activation, and (iv) decreased expression of the pluripotent marker NANOG. This then poised the cells in a potentiated state for differentiation into the three germ layers. In this state, MAT2A is upregulated, and the MTA

Figure 4. Met Deprivation Triggered Rapid Activation of p53-p38 Signaling in Pluripotent Human ESCs/iPSCs

(A) Gene expression profile analyses with undifferentiated khES3 cells showed that genes (signal intensity > 50) involved in the cell cycle or apoptosis are upregulated >3-fold in Met-deprived cells compared to cells cultured in control complete media.

(B and C) p53 expression in khES3 and 201B7 cells by western blot (B) or immunocytochemical analysis (C).

(D) The proportion of cells expressing p53 decreased with increasing Met concentration.

(E) Met deprivation, but not other amino acids, specifically increased $p53^+$ cells. SAM (100 μM) inhibited p53 accumulation in ΔMet conditions.

(F) Supplementation of 25 and 100 mM cycloleucine (CL25 and CL100) increased the number of $p53^+$ khES3 cells.

(G) p53 and phosphorylated p38 (p-p38) were upregulated 5 hr after Met deprivation in nonsilenced (NS) siRNA-treated ESCs, but neither p53 nor p-p38 increased in *p53* knockdown (KD) human ESCs.

(H) Decreased cell death in *p53* KD human ESCs after 48 hr Met deprivation.

(I) The p38 inhibitor, SB239063 (SB, 10 μM), rescued apoptosis. Error bars represent SEM (n = 3). Significant differences were determined by Student's t test; $^*p < 0.05$ and $^{**}p < 0.01$. Scale bar, 100 μm.

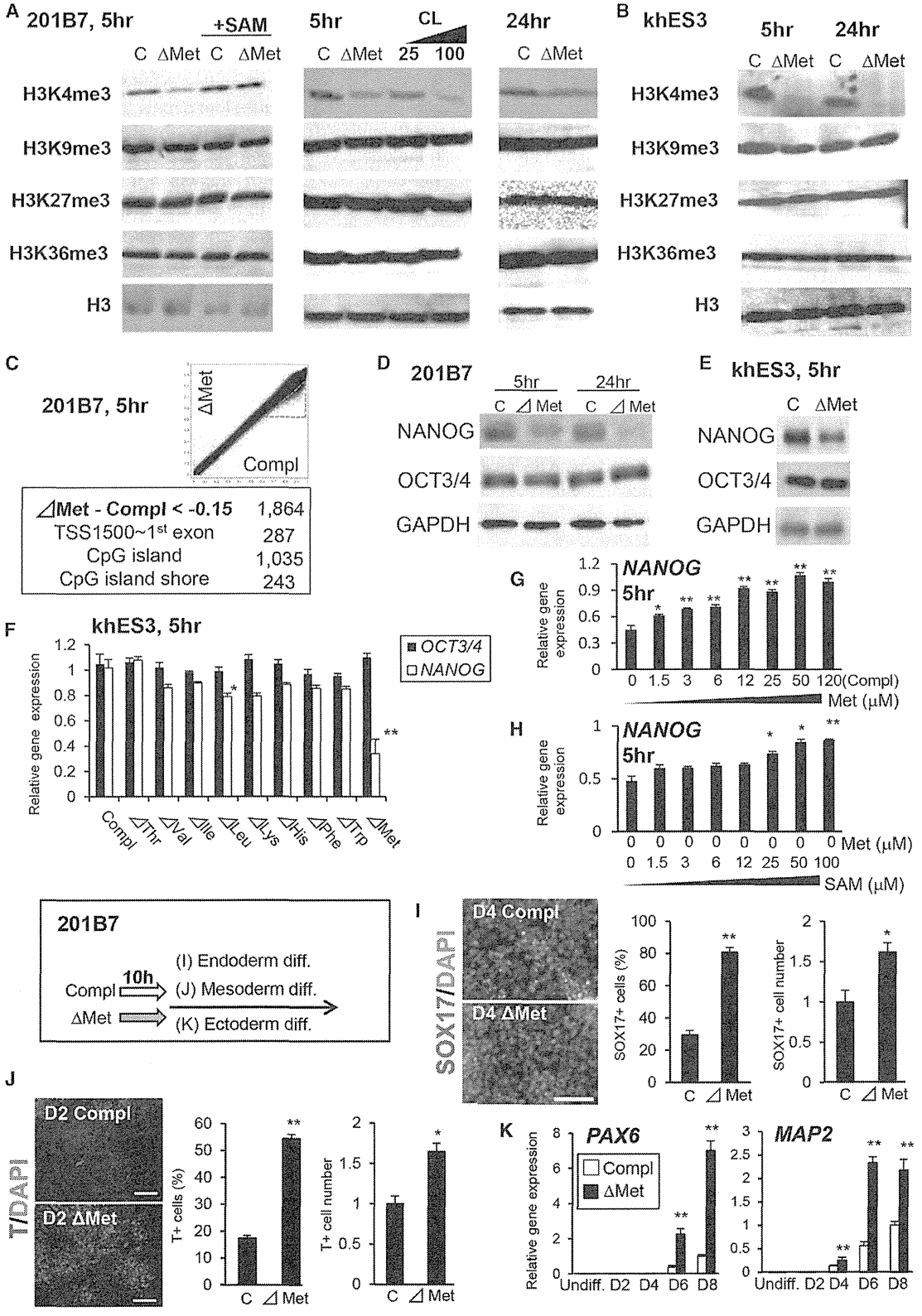

Figure 5. Short-Term Met Deprivation Triggers Histone and DNA Demethylation and Potentiates Differentiation into the Three Germ Layers

(A and B) Histone H3 methylation was examined in undifferentiated 201B7 (A) and khES3 (B) cells cultured in Met-deprived (ΔMet) or control media (C) for 5 or 24 hr. SAM supplementation (100 μM) in Met-deprived media (ΔMet+SAM) reversed demethylation of H3K4me3. Cycloleucine (100 mM) decreased H3K4me3 levels.

(legend continued on next page)

salvage pathway can replenish SAM. However, if Met depletion is prolonged and cells are not exposed to differentiation signals, the Met cycle eventually stops, and human ESCs/iPSCs undergo apoptosis.

Upon Met deprivation, cells halted excretion of Hcy and began to utilize SAM or MTA, resulting in reduced $[SAM]_i$ and $[MTA]_i$, a rapid response observed at 5 hr. *MAT2A* was upregulated to convert Met to SAM and restored the reduced $[SAM]_i$ 24 hr after Met deprivation. These events, such as salvage pathway activation and cessation of Hcy excretion, are stress responses of human ESCs/iPSCs revealed in this study. The pluripotent stem cells developed regulatory systems to maintain $[SAM]_i$ at constant levels. We also found that SAM supplementation rescued the apoptosis induced by Met deprivation, and supplementation of SAM, MTA, or Hcy rescued the impaired cell survival at a potency of SAM > MTA > Hcy. *MAT2A/MAT2B* knockdown or cycloleucine addition, but not *SMS* knockdown, phenocopied Met depletion and resulted in growth inhibition. Because cycloleucine specifically reduces $[SAM]_i$, but not $[Met]_i$, SAM, but not Met, is therefore essential for survival of undifferentiated human ESCs/iPSCs.

SAM is a major methyl donor during methyl transfer reactions, including histone or DNA methylation. Histone methylation contributes to chromatin remodeling as well as transcriptional activity (Berger, 2007). SAM functions as a sensor for Met metabolism, with a rapid decrease in $[SAM]_i$ inducing H3K4me3 and DNA demethylation, as well as decreased NANOG expression and p53-p38 pathway activation. Met deprivation rapidly poised human ESCs/iPSCs for differentiation. However, prolonged exposure to Met deprivation for 24 hr or more in the absence of appropriate differentiation signals caused the cells to undergo an irreversible change, such as prolonged G0/G1 arrest and decreased self-renewal, thus triggering apoptosis. When deprival of Met was performed during mid-stage differentiation, residual undifferentiated cells were eliminated, and overall differentiation efficiency was increased. Therefore, this knowledge is useful and applicable to eliminate variability in differentiation efficiency among cell lines and promote differentiation into specific lineages. Human iPSCs are reportedly dependent on oleate; an inhibitor of oleate synthesis shows cytotoxicity and may selectively eliminate human iPSCs (Ben-David et al., 2013). Cardiomyocytes and noncardiomyocytes from mouse and human ESCs/iPSCs differ markedly in glucose and lactate metabolism; thus, cardiomyocytes can be obtained at a high purity during large-scale purification by culture in glucose-free media (Tohyama et al., 2013). However, culture in glucose-free media did not potentiate differentiation, which differs from our present results regarding short-term Met deprivation.

While methylation of H3K4 is generally associated with activation of transcription, H3K9 and H3K27 are repressive epigenetic markers. In ESCs, simultaneous methylation of H3K4 and H3K27 is associated with the undifferentiated state, where a gene may be poised to be either fully activated or repressed (Bernstein et al., 2006). Here, decreased trimethylation of H3K4 (H3K4me3) resulting from Met deprivation suggests that Met metabolism might function in the regulation of self-renewal of pluripotent stem cells through epigenetic marking at H3K4me3 (Ang et al., 2011). Previously, mouse ESCs were reported to be in a high-flux state requiring Thr to maintain cell-cycle progression (Wang et al., 2009). In mouse ESCs, rapid conversion of Thr to Gly by Tdh is suggested to provide 5-methyltetrahydrofolate (5mTHF) needed for recycling SAH to SAM; thus, Thr deprivation caused a reduction in SAM, which then triggered demethylation of H3K4me3 and H3K4me2 (Shyh-Chang et al., 2013). In humans, the *TDH* gene is an expressed pseudogene (Edgar, 2002). Human ESCs/iPSCs directly generate SAM from Met. Therefore, mouse and human ESCs/iPSCs utilize similarly the Met pathway for maintaining their pluripotent state in principal. Met metabolism directly regulates SAM levels, and SAM reduction triggered demethylation of H3K4me3 (but not H3K9me3, H3K27me3, or H3K36me3) specifically, the mechanism of which remains unknown.

Evidence suggests that self-renewal and pluripotency are closely linked to cell-cycle regulation in pluripotent stem cells and that NANOG plays a role in the G1-to-S transition through direct binding of *CDK6* and *CDC25A* (Zhang et al., 2009). The high self-renewal rate is considered essential for maintaining ESC identity, and cell-cycle arrest is sufficient to drive human ESCs toward irreversible differentiation (Ruiz et al., 2011). Deletion of p53 in mouse cells or silencing of p53 in human somatic cells increases the reprogramming efficiency (Kawamura et al., 2009). p53 induces differentiation by directly suppressing NANOG expression in mouse ESCs (Lin et al., 2005). Our results showed that Met deprivation triggered decreased expression of NANOG, but not OCT3/4. NANOG is a member of the core transcription circuit required for ESCs to maintain pluripotency. While NANOG is actively downregulated during differentiation, OCT3/4 is downregulated when the later lineage choice occurs (Iovino and Cavalli, 2011). Our present results suggest that the Met metabolism is responsible for regulation of cell-cycle progression and maintenance of pluripotency of human ESCs/iPSCs versus differentiation or apoptosis through the p53-p38 signaling pathway. Activation of p53 signaling was observed specifically under conditions of Met deprivation but was not seen upon deprivation of other amino acids, and p53-p38 accumulation was halted by the addition of SAM.

(C) DNA methylation profiles in undifferentiated 201B7 cells cultured in complete medium (x axis) and Met-deprived medium (y axis) for 5 hr. The number of probes with greater than 15% reduction in DNA methylation under Met deprivation are shown.
(D and E) Short-term Met deprivation (5 hr) downregulated NANOG expression in 201B7 (D) and khES3 (E) cells.
(F) Real-time PCR analysis of *NANOG* and *OCT3/4* in khES3 cells in complete or amino acid-deprived media for 5 hr.
(G and H) *NANOG* expression increased with increasing Met (G) or SAM (H) concentration in the media.
(I–K) Human iPSCs cultured in Met-deprived conditions showed an elevated differentiation into the definitive endoderm (I), mesoderm (J), and ectoderm (K), as shown by expression of the endoderm marker SOX17 (I), early mesoderm marker T (J), *PAX*, or *MAP2* (K) by immunohistochemical (I and J) or real-time PCR (K) analyses. Cells were pretreated with complete medium (I and J, left bars; K, open bars) or Met-deprived media (I and J, right bars; K, black bars) before differentiation. Error bars represent SEM (n = 3). Student's t test; *$p < 0.05$ and **$p < 0.01$. Scale bar, 100 μm.

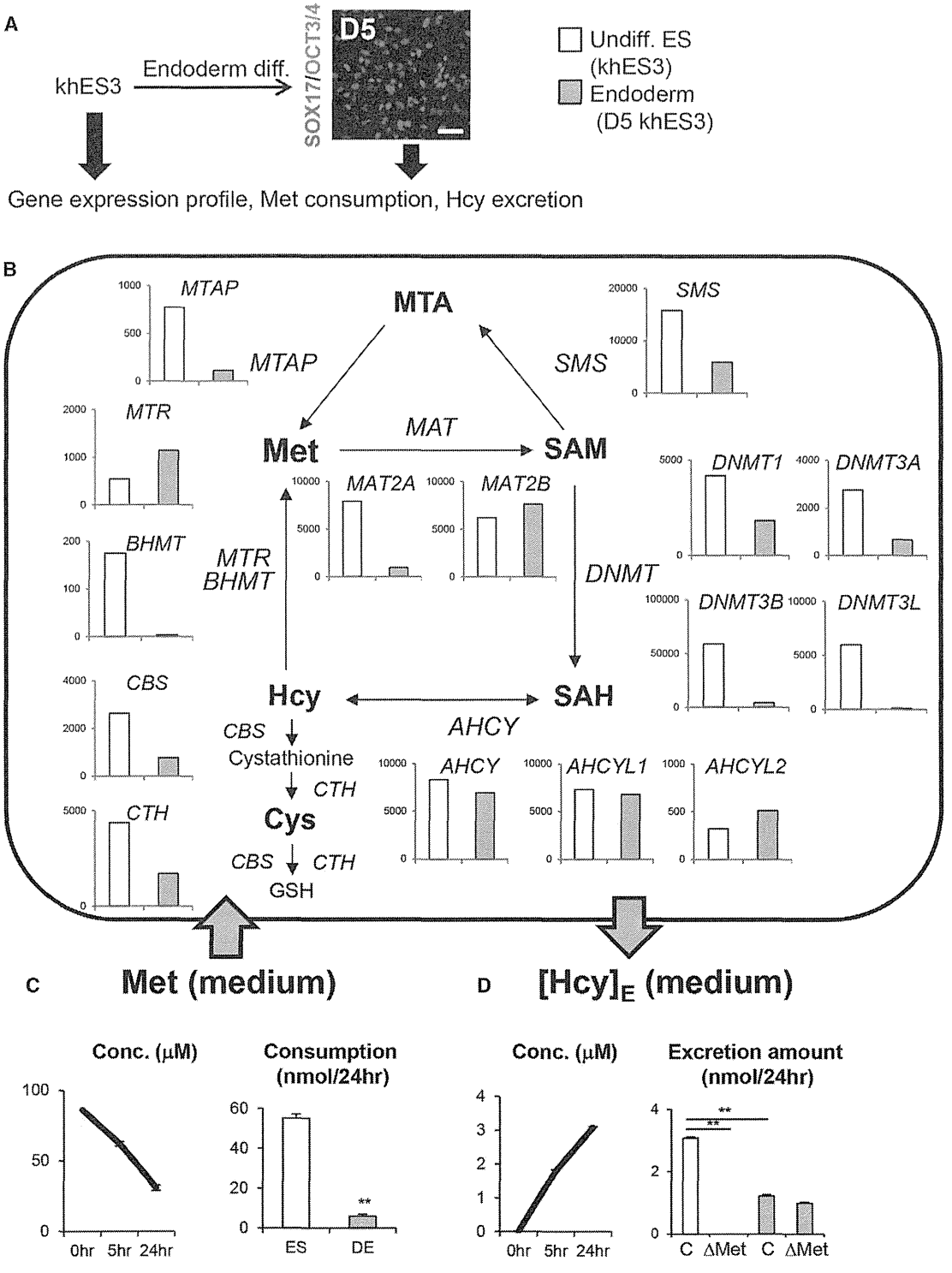

Figure 6. Undifferentiated Human ESCs Are in a High-Met Metabolic State Compared with Definitive Endoderm Cells

(A) Schematic drawings of the experimental design to determine differences in Met metabolism between undifferentiated ESCs and definitive endoderm cells. Endoderm cells differentiated for 5 days expressed SOX17, but not OCT3/4.

(B) Signal intensity of Met cycle-related genes in undifferentiated (undiff) and differentiated khES3 cells on differentiation day 5 (D5) toward the definitive endoderm analyzed by microarray.

(legend continued on next page)

SAM has been reported to act as a stress sensor in malignant cells (Lin et al., 2014). P53 is also known to trigger various stress responses (Kruse and Gu, 2009). We found that 5 hr Met deprivation in khES3 cells triggered a 27-fold increase in the expression of *EGR1*, a transcription factor that upregulates *p53* (Baron et al., 2006), or a 33-fold increase in *DHRS2*, a gene that inhibits Mdm2 and stabilizes p53 protein (Deisenroth et al., 2010). Therefore, Egr1 and DHRS2 are candidate molecules that mediate upregulation of p53 triggered by SAM limitation. However, the exact molecular mechanism linking SAM and p53 still awaits future investigations.

Taken together, our data indicate that Met deprivation results in a rapid decrease in $[SAM]_i$, triggering activation of p53-p38 signaling, reducing NANOG expression, and poising human iPSC/ESCs for differentiation. The cells endured short-term Met deprivation by replenishing the $[Met]_i$ pool with the salvage Met pathway, which was then metabolized to replenish SAM. However, during prolonged Met deprivation, the continued absence of Met metabolism led to cell-cycle arrest and apoptosis. These results are consistent with the data from previous studies indicating that p53 is a barrier to reprogramming and that decreasing p53 protein levels increases the efficiency of reprogramming (Banito et al., 2009; Kawamura et al., 2009). In conclusion, we demonstrated the importance of SAM in Met metabolism in regulating p53 signaling and its relationship with pluripotency, cell survival, and differentiation of human ESCs/iPSCs. Our findings can be utilized to eliminate undifferentiated pluripotent cells in culture and may be useful for future applications in regenerative medicine.

EXPERIMENTAL PROCEDURES

Cell Culture and Reagents

Human ESCs were approved by Kumamoto University's Institutional Review Board, following the hESC guidelines of the Japanese government. Undifferentiated human ESCs (khES1, khES3) (Suemori et al., 2006) and iPSCs (201B7, 253G1) (Takahashi et al., 2007) were maintained as described (Shiraki et al., 2008a). For feeder-free culture, ESCs/iPSCs were cultured on matrigel-coated dish with feeder-free culture media ReproFF (ReproCELL). For Met deprivation with undifferentiated cells, cells were cultured with human ESC/iPSC maintenance medium CSTI-7 (Cell Science & Technology Institute; CSTI) (Furue et al., 2008) or Met-deprived CSTI-7 medium. Met, Hcy, Cys, SAM, MTA, cycloleucine, and SAH were purchased from Sigma-Aldrich. SB239063 was purchased from Calbiochem. Methods of endoderm, mesoderm, or ectoderm differentiation, and gene knockdown examination, are described in Supplemental Experimental Procedures.

Real-Time PCR, Immunocytochemistry, and Western Blot Analysis

Real-time PCR, immunocytochemistry, and western blot were performed as previously described (Shiraki et al., 2011). Primer sequences and antibody information are shown in Tables S2 and S3, respectively. In immunocytochemical analysis, positive cells versus total cells (DAPI-positive cells) were quantified using ImageXpress Micro cellular imaging system (Molecular Devices).

Measurement of Met, SAM, SAH, MTA, and Hcy

Measurement of methionine, SAM, SAH, MTA, and Hcy was performed using ultra-high-performance liquid chromatography equipped with tandem mass spectrometry, TQD (UPLC-MS/MS; Waters) based on a previous report (Jiang et al., 2009). Separation was achieved using an ACQUITY UPLC BEH C18 column. Briefly, cells were lysed using three cycles of freeze/thaw in 50% methanol. Samples were deproteinized using 33% acetonitrile and evaporated completely. Pellets were dissolved in 10 mM HCl, followed by filtration using 0.22 μm polyvinylidene fluoride (PVDF) filter (Millipore) and diluted with equal volumes of either 50 mM Tris-HCl (pH 8.8) with 100 μm dithiothreitol (DTT) for Met, SAM, and SAH or 20 mM formic acid for MTA. For Hcy analysis in the media, cultured media were collected and incubated for 10 min at 37°C with 10 mM DTT to obtain total Hcy secreted from the cells. Media were deproteinized using 50% acetonitrile, followed by filtration, and then diluted with equal volumes of 50 mM Tris-HCl (pH 8.8). Each sample was injected, and concentrations were calculated based on the standard curve obtained from serial dilution of standard solution for each metabolite.

Microarray Analysis

Affymetrix H133 Plus 2.0 series probe array (GeneChip) was used. Expression analysis was performed using the Subio Platform (Subio).

Cell-Cycle Analysis

Fixed cells were stained with DAPI and anti-phospho Histone H3 Ser10 (pH3; Millipore). Images were acquired on the ImageXpress Micro and analyzed using the Cell Cycle Application Module (Molecular Devices).

Apoptosis Assay

Apoptosis was detected by the TUNEL method using an In Situ Cell Death Detection Kit (Roche).

Measurement of Cell Proliferation

Cell proliferation was measured by the incorporation of EdU into genomic DNA during the S phase of the cell cycle, using Click-iT EdU Kit (Invitrogen).

Functional Assays for Hepatocytes

Albumin secretion assay was performed as described (Shiraki et al., 2011). Cryopreserved human hepatocytes (Invitrogen) cultured 24 hr on collagen I coated plates with hepatocyte maintenance medium (Invitrogen) were used as positive controls.

Methylation Profiling

Methylation profiling analysis was performed as described (Nagae et al., 2011). Methylation status was analyzed using the Human Methylation 450 BeadChip (Illumina).

Statistical Analysis

Error bars represent SEM. The significance of differences between two groups was analyzed by Student's t test and presented as $^*p < 0.05$ or $^{**}p < 0.01$.

ACCESSION NUMBERS

Microarray data have been deposited under Gene Expression Omnibus (GEO) accession number GSE55285.

SUPPLEMENTAL INFORMATION

Supplemental Information includes Supplemental Experimental Procedures, four figures, and three tables and can be found with this article online at http://dx.doi.org/10.1016/j.cmet.2014.03.017.

AUTHOR CONTRIBUTIONS

N.S. and Y.S. designed the experiments and performed cellular and biochemical analyses to check the effect of Met in differentiation stages. N.S.

(C) Time-dependent changes in Met concentration 5 or 24 hr after culture in complete media (left). Met consumption at 24 hr in undifferentiated or endoderm cells (right).

(D) Time-dependent excretion of Hcy 5 or 24 hr after culture in complete media. Excreted Hcy ($[Hcy]_E$) at 24 hr in undifferentiated or endoderm cells grown in complete or Met-deprived media. Error bars represent SEM (n = 3). Student's t test; $^{**}p < 0.01$. Scale bar, 100 μm. Open bars, undifferentiated cells; gray bars, definitive endoderm.

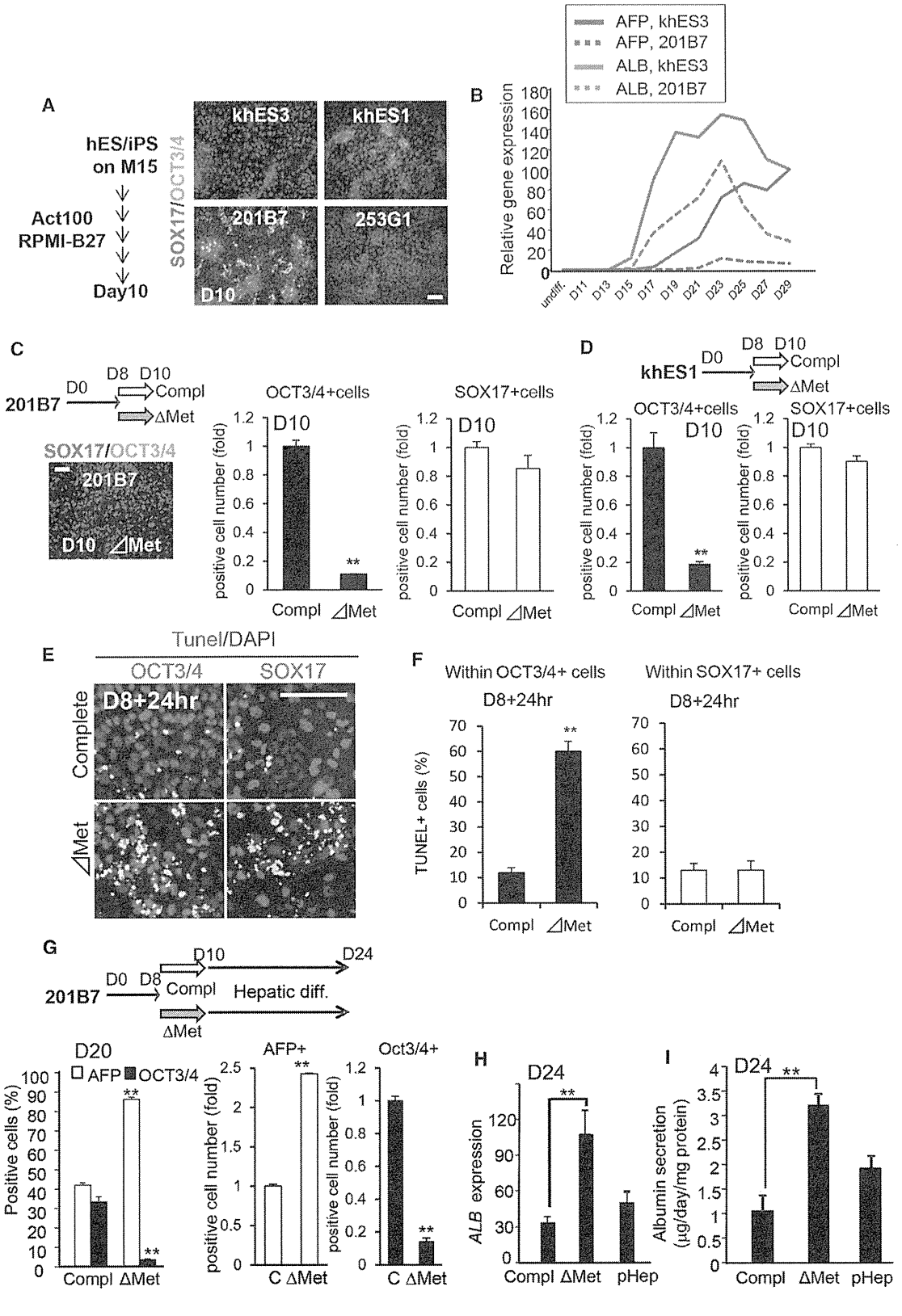

(legend on next page)

performed cellular and biochemical analyses to check the effect of Met in the undifferentiation stage and wrote the paper. T.T. handled the collection and assembly of data. F.O. and M.M. performed the measurement of Met-cycle metabolites. G.N. and H.A. performed the analysis of global DNA methylation. K.K. provided technical advice and helpful discussions. F.E. conceived the study and provided technical advice and financial support. S.K. conceived the study and design, wrote the paper, interpreted results, provided financial support, and finalized the manuscript.

ACKNOWLEDGMENTS

We thank Drs. Norio Nakatsuji and Hirofumi Suemori (Kyoto University) for providing khES1 and khES3 cells and Dr. Shinya Yamanaka (Kyoto University) for providing 201B7 and 253G1 iPSC lines. We thank Ms. Nigar Sultana, Akiko Harada, and the members of the Gene Technology Center at Kumamoto University for their technical assistance. This work was supported by a grant from the National Institute of Biomedical Innovation (to N.S.); the NEXT Program (to S.K.) by the Japanese Society for the Promotion of Science (JSPS); and a grant from the Project for Realization of Regenerative Medicine from the Ministry of Education, Culture, Sports, Science and Technology (MEXT) Japan (to S.K. and F.E.). This work was also supported in part by the Program for Leading Graduate Schools "HIGO (Health life science; Interdisciplinary and Glocal Oriented) Program" (to S.K.), from MEXT. S.K. is a member of the Program for Leading Graduate Schools "HIGO."

Received: September 22, 2013
Revised: January 9, 2014
Accepted: March 11, 2014
Published: April 17, 2014

REFERENCES

Alexander, P.B., Wang, J., and McKnight, S.L. (2011). Targeted killing of a mammalian cell based upon its specialized metabolic state. Proc. Natl. Acad. Sci. USA *108*, 15828–15833.

Ang, Y.S., Tsai, S.Y., Lee, D.F., Monk, J., Su, J., Ratnakumar, K., Ding, J., Ge, Y., Darr, H., Chang, B., et al. (2011). Wdr5 mediates self-renewal and reprogramming via the embryonic stem cell core transcriptional network. Cell *145*, 183–197.

Armstrong, L., Tilgner, K., Saretzki, G., Atkinson, S.P., Stojkovic, M., Moreno, R., Przyborski, S., and Lako, M. (2010). Human induced pluripotent stem cell lines show stress defense mechanisms and mitochondrial regulation similar to those of human embryonic stem cells. Stem Cells *28*, 661–673.

Banito, A., Rashid, S.T., Acosta, J.C., Li, S., Pereira, C.F., Geti, I., Pinho, S., Silva, J.C., Azuara, V., Walsh, M., et al. (2009). Senescence impairs successful reprogramming to pluripotent stem cells. Genes Dev. *23*, 2134–2139.

Baron, V., Adamson, E.D., Calogero, A., Ragona, G., and Mercola, D. (2006). The transcription factor Egr1 is a direct regulator of multiple tumor suppressors including TGFbeta1, PTEN, p53, and fibronectin. Cancer Gene Ther. *13*, 115–124.

Ben-David, U., Gan, Q.F., Golan-Lev, T., Arora, P., Yanuka, O., Oren, Y.S., Leikin-Frenkel, A., Graf, M., Garippa, R., Boehringer, M., et al. (2013). Selective elimination of human pluripotent stem cells by an oleate synthesis inhibitor discovered in a high-throughput screen. Cell Stem Cell *12*, 167–179.

Berger, S.L. (2007). The complex language of chromatin regulation during transcription. Nature *447*, 407–412.

Bernstein, B.E., Mikkelsen, T.S., Xie, X., Kamal, M., Huebert, D.J., Cuff, J., Fry, B., Meissner, A., Wernig, M., Plath, K., et al. (2006). A bivalent chromatin structure marks key developmental genes in embryonic stem cells. Cell *125*, 315–326.

Boheler, K.R. (2009). Stem cell pluripotency: a cellular trait that depends on transcription factors, chromatin state and a checkpoint deficient cell cycle. J. Cell. Physiol. *221*, 10–17.

Bruhat, A., Jousse, C., Wang, X.Z., Ron, D., Ferrara, M., and Fafournoux, P. (1997). Amino acid limitation induces expression of CHOP, a CCAAT/enhancer binding protein-related gene, at both transcriptional and post-transcriptional levels. J. Biol. Chem. *272*, 17588–17593.

Deisenroth, C., Thorner, A.R., Enomoto, T., Perou, C.M., and Zhang, Y. (2010). Mitochondrial Hep27 is a c-Myb target gene that inhibits Mdm2 and stabilizes p53. Mol. Cell. Biol. *30*, 3981–3993.

Edgar, A.J. (2002). The human L-threonine 3-dehydrogenase gene is an expressed pseudogene. BMC Genet. *3*, 18.

Facucho-Oliveira, J.M., and St John, J.C. (2009). The relationship between pluripotency and mitochondrial DNA proliferation during early embryo development and embryonic stem cell differentiation. Stem Cell Rev. *5*, 140–158.

Finkelstein, J.D. (1990). Methionine metabolism in mammals. J. Nutr. Biochem. *1*, 228–237.

Folmes, C.D., Nelson, T.J., Martinez-Fernandez, A., Arrell, D.K., Lindor, J.Z., Dzeja, P.P., Ikeda, Y., Perez-Terzic, C., and Terzic, A. (2011). Somatic oxidative bioenergetics transitions into pluripotency-dependent glycolysis to facilitate nuclear reprogramming. Cell Metab. *14*, 264–271.

Furue, M.K., Na, J., Jackson, J.P., Okamoto, T., Jones, M., Baker, D., Hata, R., Moore, H.D., Sato, J.D., and Andrews, P.W. (2008). Heparin promotes the growth of human embryonic stem cells in a defined serum-free medium. Proc. Natl. Acad. Sci. USA *105*, 13409–13414.

Goll, M.G., and Bestor, T.H. (2005). Eukaryotic cytosine methyltransferases. Annu. Rev. Biochem. *74*, 481–514.

Halim, A.B., LeGros, L., Geller, A., and Kotb, M. (1999). Expression and functional interaction of the catalytic and regulatory subunits of human methionine adenosyltransferase in mammalian cells. J. Biol. Chem. *274*, 29720–29725.

Iovino, N., and Cavalli, G. (2011). Rolling ES cells down the Waddington landscape with Oct4 and Sox2. Cell *145*, 815–817.

Iwashita, H., Shiraki, N., Sakano, D., Ikegami, T., Shiga, M., Kume, K., and Kume, S. (2013). Secreted cerberus1 as a marker for quantification of definitive endoderm differentiation of the pluripotent stem cells. PLoS ONE *8*, e64291.

Jiang, Z., Liang, Q., Luo, G., Hu, P., Li, P., and Wang, Y. (2009). HPLC-electrospray tandem mass spectrometry for simultaneous quantitation of eight plasma aminothiols: application to studies of diabetic nephropathy. Talanta *77*, 1279–1284.

Kajiwara, M., Aoi, T., Okita, K., Takahashi, R., Inoue, H., Takayama, N., Endo, H., Eto, K., Toguchida, J., Uemoto, S., and Yamanaka, S. (2012). Donor-dependent variations in hepatic differentiation from human-induced pluripotent stem cells. Proc. Natl. Acad. Sci. USA *109*, 12538–12543.

Figure 7. Met Deprivation Potentiates Hepatic Differentiation

(A) khES1, khES3, 201B7, and 253G1 cells were subjected to endodermal differentiation using M15 feeder cells (Shiraki et al., 2008a; Umeda et al., 2013). SOX17 (red) and OCT3/4 (green) expression was detected by immunocytochemistry.

(B) *AFP* (red) or *ALB* (blue) mRNA expression was detected by real-time PCR. Expression in khES3 (solid lines) or 201B7 cells (broken lines).

(C and D) Impact of Met deprivation on the remaining $OCT3/4^+$ undifferentiated cells (black bars) or $SOX17^+$ definitive endoderm cells (open bars) derived from 201B7 cells (C) or khES1 cells (D).

(E) Fluorescent image of TUNEL staining.

(F) Quantitative analysis of TUNEL-positive cells.

(G–I) The impact of Met deprivation on hepatic differentiation. (G) Proportions and number of AFP^+ cells (open bars) or $OCT3/4^+$ cells (black bars) in complete or Met-deprived media. (H and I) Upon Met deprivation, increased *ALB* expression (H) and ALB secretion on D24 (I) were observed. pHep, primary human hepatocytes. Error bars represent SEM (n = 3). Significant differences were determined by Student's t test; $^{**}p < 0.01$. Scale bar, 100 μm.

Kawamura, T., Suzuki, J., Wang, Y.V., Menendez, S., Morera, L.B., Raya, A., Wahl, G.M., and Izpisúa Belmonte, J.C. (2009). Linking the p53 tumour suppressor pathway to somatic cell reprogramming. Nature *460*, 1140–1144.

Kruse, J.P., and Gu, W. (2009). Modes of p53 regulation. Cell *137*, 609–622.

Lin, T., Chao, C., Saito, S., Mazur, S.J., Murphy, M.E., Appella, E., and Xu, Y. (2005). p53 induces differentiation of mouse embryonic stem cells by suppressing Nanog expression. Nat. Cell Biol. *7*, 165–171.

Lin, D.W., Chung, B.P., and Kaiser, P. (2014). S-adenosylmethionine limitation induces p38 mitogen-activated protein kinase and triggers cell cycle arrest in G1. J. Cell Sci. *127*, 50–59.

Lu, S.C., and Mato, J.M. (2008). S-Adenosylmethionine in cell growth, apoptosis and liver cancer. J. Gastroenterol. Hepatol. *23* (*Suppl 1*), S73–S77.

Nagae, G., Isagawa, T., Shiraki, N., Fujita, T., Yamamoto, S., Tsutsumi, S., Nonaka, A., Yoshiba, S., Matsusaka, K., Midorikawa, Y., et al. (2011). Tissue-specific demethylation in CpG-poor promoters during cellular differentiation. Hum. Mol. Genet. *20*, 2710–2721.

Ogaki, S., Shiraki, N., Kume, K., and Kume, S. (2013). Wnt and Notch signals guide embryonic stem cell differentiation into the intestinal lineages. Stem Cells *31*, 1086–1096.

Osafune, K., Caron, L., Borowiak, M., Martinez, R.J., Fitz-Gerald, C.S., Sato, Y., Cowan, C.A., Chien, K.R., and Melton, D.A. (2008). Marked differences in differentiation propensity among human embryonic stem cell lines. Nat. Biotechnol. *26*, 313–315.

Oyadomari, S., and Mori, M. (2004). Roles of CHOP/GADD153 in endoplasmic reticulum stress. Cell Death Differ. *11*, 381–389.

Ruiz, S., Panopoulos, A.D., Herrerías, A., Bissig, K.D., Lutz, M., Berggren, W.T., Verma, I.M., and Izpisua Belmonte, J.C. (2011). A high proliferation rate is required for cell reprogramming and maintenance of human embryonic stem cell identity. Curr. Biol. *21*, 45–52.

Shi, Y. (2007). Histone lysine demethylases: emerging roles in development, physiology and disease. Nat. Rev. Genet. *8*, 829–833.

Shiraki, N., Umeda, K., Sakashita, N., Takeya, M., Kume, K., and Kume, S. (2008a). Differentiation of mouse and human embryonic stem cells into hepatic lineages. Genes Cells *13*, 731–746.

Shiraki, N., Yoshida, T., Araki, K., Umezawa, A., Higuchi, Y., Goto, H., Kume, K., and Kume, S. (2008b). Guided differentiation of embryonic stem cells into Pdx1-expressing regional-specific definitive endoderm. Stem Cells *26*, 874–885.

Shiraki, N., Yamazoe, T., Qin, Z., Ohgomori, K., Mochitate, K., Kume, K., and Kume, S. (2011). Efficient differentiation of embryonic stem cells into hepatic cells in vitro using a feeder-free basement membrane substratum. PLoS ONE *6*, e24228.

Shyh-Chang, N., Locasale, J.W., Lyssiotis, C.A., Zheng, Y., Teo, R.Y., Ratanasirintrawoot, S., Zhang, J., Onder, T., Unternaehrer, J.J., Zhu, H., et al. (2013). Influence of threonine metabolism on S-adenosylmethionine and histone methylation. Science *339*, 222–226.

Suemori, H., Yasuchika, K., Hasegawa, K., Fujioka, T., Tsuneyoshi, N., and Nakatsuji, N. (2006). Efficient establishment of human embryonic stem cell lines and long-term maintenance with stable karyotype by enzymatic bulk passage. Biochem. Biophys. Res. Commun. *345*, 926–932.

Sufrin, J.R., Coulter, A.W., and Talalay, P. (1979). Structural and conformational analogues of L-methionine as inhibitors of the enzymatic synthesis of S-adenosyl-L-methionine. IV. Further mono-, bi- and tricyclic amino acids. Mol. Pharmacol. *15*, 661–677.

Takahashi, K., Tanabe, K., Ohnuki, M., Narita, M., Ichisaka, T., Tomoda, K., and Yamanaka, S. (2007). Induction of pluripotent stem cells from adult human fibroblasts by defined factors. Cell *131*, 861–872.

Takubo, K., Nagamatsu, G., Kobayashi, C.I., Nakamura-Ishizu, A., Kobayashi, H., Ikeda, E., Goda, N., Rahimi, Y., Johnson, R.S., Soga, T., et al. (2013). Regulation of glycolysis by Pdk functions as a metabolic checkpoint for cell cycle quiescence in hematopoietic stem cells. Cell Stem Cell *12*, 49–61.

Tohyama, S., Hattori, F., Sano, M., Hishiki, T., Nagahata, Y., Matsuura, T., Hashimoto, H., Suzuki, T., Yamashita, H., Satoh, Y., et al. (2013). Distinct metabolic flow enables large-scale purification of mouse and human pluripotent stem cell-derived cardiomyocytes. Cell Stem Cell *12*, 127–137.

Umeda, K., Suzuki, K., Yamazoe, T., Shiraki, N., Higuchi, Y., Tokieda, K., Kume, K., Mitani, K., and Kume, S. (2013). Albumin gene targeting in human embryonic stem cells and induced pluripotent stem cells with helper-dependent adenoviral vector to monitor hepatic differentiation. Stem Cell Res. (Amst.) *10*, 179–194.

Wang, J., Alexander, P., Wu, L., Hammer, R., Cleaver, O., and McKnight, S.L. (2009). Dependence of mouse embryonic stem cells on threonine catabolism. Science *325*, 435–439.

Wellen, K.E., and Thompson, C.B. (2012). A two-way street: reciprocal regulation of metabolism and signalling. Nat. Rev. Mol. Cell Biol. *13*, 270–276.

Zhang, X., Neganova, I., Przyborski, S., Yang, C., Cooke, M., Atkinson, S.P., Anyfantis, G., Fenyk, S., Keith, W.N., Hoare, S.F., et al. (2009). A role for NANOG in G1 to S transition in human embryonic stem cells through direct binding of CDK6 and CDC25A. J. Cell Biol. *184*, 67–82.

SCIENTIFIC REPORTS

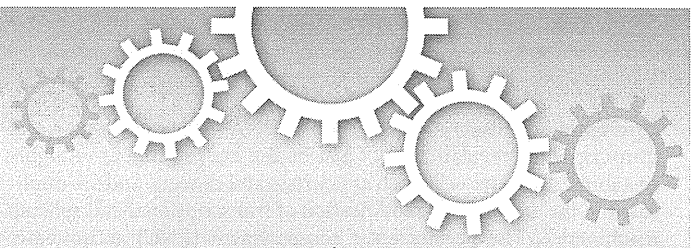

OPEN

SUBJECT AREAS:
INDUCED PLURIPOTENT STEM CELLS
IMAGE PROCESSING
NUCLEAR ORGANIZATION

Received
19 June 2014

Accepted
22 October 2014

Published
11 November 2014

Correspondence and requests for materials should be addressed to N.S. (norikos@kumamoto-u.ac.jp) or M.N. (mnakao@gpo.kumamoto-u.ac.jp)

Computational image analysis of colony and nuclear morphology to evaluate human induced pluripotent stem cells

Kazuaki Tokunaga[1,2], Noriko Saitoh[1,2], Ilya G. Goldberg[3], Chiyomi Sakamoto[1], Yoko Yasuda[1], Yoshinori Yoshida[4], Shinya Yamanaka[4,5] & Mitsuyoshi Nakao[1,2]

[1]Department of Medical Cell Biology, Institute of Molecular Embryology and Genetics, Kumamoto University, 2-2-1 Honjo, Chuo-ku, Kumamoto 860-0811, Japan, [2]Core Research for Evolutional Science and Technology (CREST), Japan Science and Technology Agency, Tokyo, Japan, [3]Image Informatics and Computational Biology Unit, Laboratory of Genetics, National Institute on Aging, National Institutes of Health, 251 Bayview Boulevard, Suite 100, Baltimore, MD 21224, USA, [4]Center for iPS Cell Research and Application, Kyoto University, 53 Shogoin-Kawaharacho, Sakyo-ku, Kyoto, 606-8507, Japan, [5]Gladstone Institute of Cardiovascular Disease, 1650 Owens Street, San Francisco, CA 94158, USA.

Non-invasive evaluation of cell reprogramming by advanced image analysis is required to maintain the quality of cells intended for regenerative medicine. Here, we constructed living and unlabelled colony image libraries of various human induced pluripotent stem cell (iPSC) lines for supervised machine learning pattern recognition to accurately distinguish bona fide iPSCs from improperly reprogrammed cells. Furthermore, we found that image features for efficient discrimination reside in cellular components. In fact, extensive analysis of nuclear morphologies revealed dynamic and characteristic signatures, including the linear form of the promyelocytic leukaemia (PML)-defined structure in iPSCs, which was reversed to a regular sphere upon differentiation. Our data revealed that iPSCs have a markedly different overall nuclear architecture that may contribute to highly accurate discrimination based on the cell reprogramming status.

The generation of human induced pluripotent stem cells (iPSCs) is simple and highly reproducible[1]. However, only a small proportion of cells become pluripotent after introduction of the reprogramming factors, possibly resulting in a mixture of bona fide iPSCs and partially reprogrammed cells[2,3]. It is essential to develop reliable methods to select completely reprogrammed iPSCs by eliminating the contamination of non-iPSCs[4]. Previous studies have shown changes in gene expression, DNA methylation, and histone modifications during iPSC reprogramming[1,5]. Furthermore, reporter genes have been integrated into the genomic loci of pluripotency genes to visualize bona fide iPSCs[4]. However, there are no non-invasive methods that reliably identify live human iPSCs in large and heterogeneous populations of reprogramming cells.

Recent advances in automated biological image analyses enable objective measurements of cellular morphologies[6]. A supervised machine learning algorithm, wndchrm (weighted neighbour distances using a compound hierarchy of algorithms representing morphology), has been developed for automated image classification and mining of image similarities or differences[7]. It is a flexible, multi-purpose image classifier that can be applied to a wide range of bio-image problems. Unlike conventional image analysis, where users are required to specify target morphologies, choose specific algorithms, and try different parameters depending on the imaging problem, wndchrm users define classes by providing example images for each class; completely reprogrammed cells or partially reprogrammed cells, for example. Once classes are defined, classifications and similarity measurements are performed automatically. As the first step of the classification, wndchrm computes a large set of image features for each image in the defined classes and then selects image features that are informative for discrimination of the groups and constructs a classifier in an automated fashion[6,7]. Next, the dataset is tested by multiple rounds of cross validation to measure classification accuracy (CA) as well as class similarity, which can be visualized with phylogenetic tree. The wndchrm algorithm has been successfully used for early detection of osteoarthritis[8], measurement of muscle decline with aging, sarcopenia[9], classification of malignant lymphoma[10], and many other applications[10].

Nuclear structure and function are closely linked to cellular reprogramming and epigenomic regulation[5]. During cell differentiation, nuclear structures are reconfigured dynamically. Previous studies have identified numerous distinct nuclear bodies[11–13]. For example, promyelocytic leukaemia (PML) nuclear bodies typically exist as small spheres of 0.3–1.0 μm in diameter, and are implicated in various cellular pathways including

chromatin organisation, viral response, DNA replication, repair, and transcriptional regulation[11,13]. Cajal Bodies are prominent in highly metabolically active cells such as neurons and cancers, and are implicated in the assembly or modification of transcriptional and splicing machinery[14]. The perinucleolar compartment (PNC) accumulates polypyrimidine tract binding protein[15] and several polymerase III RNAs, which appears in virtually all types of solid tumours[16]. These bodies have been studied intensively in somatic cells[11–13], but much less is known about them in human iPSCs[17].

Here, we established an accurate classification method to identify iPSCs using images of unlabelled live iPSC colonies. A combination of wndchrm and specific morphology quantification suggested that signals contributing to morphological discrepancies reside in nuclear sub-domains.

Results

Colony morphologies reflect proper reprogramming, which can be measured by pattern recognition. To build image classifiers to differentiate variously reprogrammed human cells, we first collected phase contrast images of live colonies formed by standard iPSC lines (201B7 and 253G1)[2,3], newly generated iPSC lines (1H–4H), non-iPSC lines (15B2 and 2B7), and somatic cells (human mammary epithelial cells, HMECs) (Fig. 1a). 253G1 and 201B7 cells were the initially established iPSC lines that were generated from human fibroblasts by introduction of four factors (Oct3/4, Sox2, Klf4, and c-Myc) and three factors (Oct3/4, Sox2, and Klf4), respectively[2,3]. New iPSCs and non-iPSCs were derived from HMECs and human fibroblasts by a Sendai virus (SeV) carrying the four factors[18]. We confirmed that these iPSCs maintained pluripotency and could differentiate into three lineages *in vitro* (Supplementary Figs. S1 and S2)[2,3]. In contrast, 15B2 and 2B7 cells lacked pluripotency, probably because of failure to silence the transgenes and activate endogenous stemness genes[1]. The resultant image libraries included 60 colony images (1024 × 767 pixels) for each of the nine cell lines (Supplementary Fig. S3). In wndchrm, pattern recognition is based on ability to distinguish different classes, not pre-defined objects. Therefore, other than manually centering colonies, we used the entire colony image with no prior segmentation, as input.

The image classifier must be trained with a sufficient number of images. To optimize the classification capacities, we measured CA using different number of training data set of iPSC (1H) and non-iPSC (15B2), and found that the accuracy reached a plateau with more than 40 images (Supplementary Fig. S4a).

In addition, dividing a large image into multiple equal-sized tiles can sometimes provide better classification, particularly when numerous cells are distributed throughout an image. Treating the tilled images independently is expected to improve classification ability as the size of dataset increases[19,20]. Therefore, we measured CA with and without tiling and found that the accuracy was improved by breaking an image into more than 16 images (Supplementary Fig. S4b).

Under these optimized classification condition, we classified several cell lines against iPSCs (1H cells) and compared CAs (Fig. 1b). In this binary classification, CA reflects the degree of morphological dissimilarities[7]. If the morphologies of two cell types are very distinct, the classifier is expected to show higher rate of accurate cross validations, at the maximum CA of 1. 0. On the other hand, the CA value of random classification between two cell types with no feature differences is expected to be 0.5. The results showed that the CA against iPSCs (1H cells) was 0.66 for 2H cells, 0.68 for 201B7 cells, and 0.63 for 253G1 cells, but it was significantly high for non-iPSCs, 15B2 cells (0.87), and HMECs (0.96) (Fig. 1b). Therefore, wndchrm analysis was effective for discrimination of iPSC and non-iPSC colonies.

A set of informative image features extracted from each wndchrm test is summarized in Figure 1c and Supplementary Table S1. The Fisher discriminant values were clearly small between iPSC lines (1H vs. 2H, and 1H vs. 201B7), while they were remarkably large for non-iPSCs (15B2 cells) and HMECs that exhibited a common feature pattern (Fig. 1c). In addition, most of the image features that contributed to the accurate classifications were based on transformed images (Fig. 1c, black bars)[6,7]. Thus, wndchrm analyses are effective and objective for discrimination of iPSC and non-iPSC colonies.

We further examined the morphological similarities among the cell lines. The phylogeny in Fig. 1d was generated based on the pairwise class similarity (Supplementary Table S2), and showed that various iPSC lines, particularly those reprogrammed with the four factors, were closely clustered, whereas non-iPSCs (15B2) and HMECs were distantly positioned from them (Fig. 1d, and Supplementary Figs. S4c and S4d). A set of most informative image features extracted for this wndchrm test is listed in Supplementary Table S4.

Consistently, classifications between any combination of iPSC lines (1H-4H) resulted in low CA, which suggests that their morphologies are similar to each other (Supplementary Fig. S4e). Furthermore, binary classifications using another iPSC line (4H) as a reference (Supplementary Fig. S4f) resulted in a similar pattern to Fig. 1b.

Besides the above-mentioned studies on the cell lines, wndchrm analysis was effective to classify partially reprogrammed and fully reprogrammed mouse cells grown in the same dish as a mixed population (Supplementary Fig. S5).

Reprogrammed cells grow as large colonies. We investigated the nature of image features that discriminate iPSCs and non iPSCs. As mentioned above, we classified iPSCs (1H) and non-iPSCs (15B2) with and without tiling the colony images (Supplementary Fig. S4b). By doing so, an image is broken into equally sized rectangles that are treated independently for successive training and test. An important feature as a single entity is lost, while the one distributed throughout the image is maintained, and size of the data set increases. We found that the CA was improved by tiling (Supplementary Fig. S4b), suggesting that the signals to identify iPSCs (1H) and non-iPSCs (15B2) were scattered in the image, and the colony morphology *per se* is not critical.

We further localised image features that discriminate iPSCs (1H) and non-iPSC (15B2) by tiling the colony images into 64 tiles and measuring the CA in each of them (Fig. 1e). As expected, a large part of the predictive signal came from areas containing iPSCs. Interestingly, the higher signals (CA ≥ 0.75) were positioned inside of the colony region (Inside), rather than the periphery with the local edge shape (Periphery) or outside of the colony (MEF), suggesting that unique features of the internal structure of the colony contribute most to the distinction.

Because nuclear morphology changes during differentiation status[21–23], we searched nuclear sub-structures that are different in iPSCs and non-iPSCs. Among the nuclear structures tested in this study, lamin A/C, the major component of the nuclear lamina[24], was expressed in the peripheral cells of iPSC colonies, while it was detected in most of the cells in non-iPSC colonies (Fig. 1f). In addition, transcription factor Sp1 (specificity protein 1)[25] was highly expressed inside of iPSC colonies (Supplementary Fig. S6). Such a metastatic state of iPSCs in the colony may be recognized by wndchrm.

The linear form of the PML-defined structure is characteristic of appropriately reprogrammed iPSCs. Extensive immunofluorescence analyses of ~20 distinct nuclear structures revealed that the PML body[26,27], Cajal body[27], and PNC[27] were characteristic of bona fide iPSCs, non-iPSCs, and cancerous HeLa cells, respectively (Figs. 2a–b, and Supplementary Fig. S7). The frequency of PML body formation in iPSC lines (1H, 201B7, and 253G1) was less than that in non-iPSC lines (15B2 and 2B7), and somatic cell lines (HMECs and IMR90 fibroblasts). Cajal body formation in non-iPSCs (0 ± 0.2 per

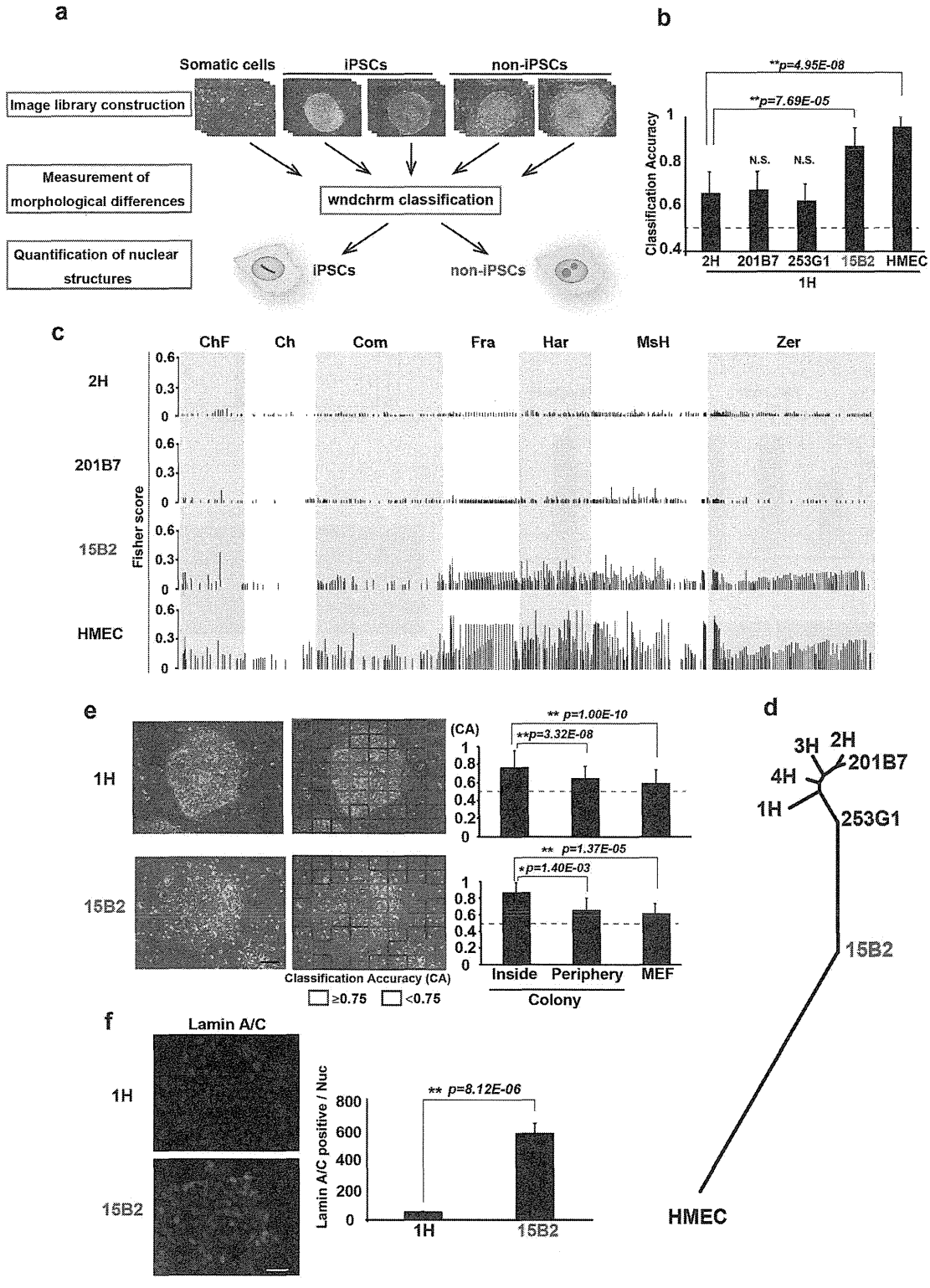

Figure 1 | Quantitative classification of completely and incompletely reprogrammed human iPSC colonies. (a) Experimental Overview. iPSCs and non-iPSCs are indicated as blue and red, respectively. (b) Binary classification of colony images against iPSCs (1H). Classification accuracy (CA) indicates the level of morphological differences between two cell types. CA value of two cell types with no feature differences is expected to be 0.5 (dotted line). The values are the means and standard deviation (s.d.) from 10 independent tests. N.S., not significant. (c) Fisher discriminant scores assigned to the 2873 features for each test in Fig. 1b. The values were calculated from raw (red bars) and transformed images (black bars). The name of each feature group is described in Supplementary Table S1. (d) Phylogeny based on morphological similarities. (e) Specification of the areas that distinguish iPSC (1H) and non-iPSC (15B2) colonies. CA values for each sub-image are shown as high (red) and low (blue). Average CA values inside, at the periphery, and outside of the colony (MEF, mouse embryonic fibroblast) are shown on the graph. (f) Selective expression of lamin A/C in the periphery of the iPSC colony. Immunofluorescence images of lamin A/C (green) and DAPI (blue), and quantified intensities are shown at the right (n>600). Values are the means and s.d. *, $p<0.05$; **, $p<0.01$. Scale bars, 200 μm.